Holocene climate dynamics on the European scale: Insights from a coastal archaeological record from the temperate Bay of Biscay (SW France)

Frederique Eynaud, Florence Verdin, Yannick Mary, Celia Beaudouin, Elias Lopez-Romero, Aurelie Penaud, Christophe Colin, Camile Culioli

Holocene climate dynamics on the European scale: Insights from a coastal archaeological record from the temperate Bay of Biscay (SW France)

Frédérique Eynaud[a,*], Florence Verdin[b], Yannick Mary[a], Célia Beaudoin[c], Elías López-Romero[d], Aurélie Penaud[e], Christophe Colin[f], Camile Culioli[b]

[a] Université de Bordeaux, CNRS, EPOC, EPHE, UMR 5805, F-33600 Pessac, France

[b] Laboratoire AUSONIUS, 8, esplanade des Antilles, F-33607 PESSAC, France

[c] Pollen core, France

[d] Universidad Complutense de Madrid, Dpto. de Prehistoria, Hª Antigua y Arqueología, 28040 Madrid, Spain

[e] Laboratoire Domaines Océaniques, IUEM, Université de Brest, F-29280, PLOUZANE, France

[f] Université Paris-Saclay, CNRS, GEOPS, 91405, Orsay, France

* *Corresponding author.*

E-mail address: *frederique.eynaud@u-bordeaux.fr* (F. Eynaud).

ABSTRACT

The main drivers of Europe's climate during the Holocene result from the coupling and interplay of external and internal radiative processes with the shifting patterns of many dynamic components (e.g. glaciers, ocean currents, wind fields, vegetation cover). Those driving forces were expressed across a range of geographical scales, from local to global, in a diverse set of records forming a patchwork of evidence as to the fundamental pacing effect of climate on past ecosystems. Various sedimentary deposits resulting from those complex forcing contexts bear climatic signatures that it is not always easy to disentangle especially with respect to local factors.

The present paper focuses on a coastal archaeological site on the Medoc peninsula (the Lède du Gurp site in south-western France) that records Holocene palaeoenvironmental changes, decoded here century after century and integrated with ongoing events on a pan-North-Atlantic scale. Based on updated geoarchaeological approaches, thanks to new applications of proxies, especially X-ray fluorescence (XRF) core scanning methods for this article, continuous sedimentary records have been analysed in order to reconstruct a regional framework for past ecosystem events, including events potentially related to human activity. Our work identifies signals on various scales in the record under study, with both long- and short-term trends and local and global imprints, but all closely bound up with proximal North Atlantic Ocean dynamics. It highlights how western European environments (and so populations) were dependent upon the linearity of climate evolution at the key Northgrippian/Meghalayan transition.

KEYWORDS

Holocene; Neolithic; Climate dynamics; North Atlantic Ocean; Sea-surface conditions

1. Introduction

The question of the climatic determinism of the evolution of human societies is still much debated in the scientific community. However, throughout the Holocene (last ~11.7 ka cal BP, e.g. Walker et al., 2019 and references therein), much evidence points to a close connection between human behaviour (e.g. habitats, techniques, cultures, practices) and climatic conditions (e.g. de Menocal, 2001; Ruddiman and Thomson, 2001; Mayewski et al., 2004; Ruddiman et al., 2016). The increase in the number of human settlements largely coincides with the onset of the mid-Holocene (6–7 ka BP) when the melting of boreal glaciers, global temperatures and sea level all stabilized (from Jansen and Bjørklund, 1985 to Eynaud et al., 2018 and references therein). Those events are related to well-known climatic subdivisions, with the termination of the warm (hypsithermal) Atlantic period (e.g. Jansen and Bjørklund, 1985), recently included within the Northgrippian stage (e.g. Walker et al., 2019), and corresponding to the cultural Mesolithic-Neolithic transition in Western Europe. The Anthropocene, *sensu lato* (i.e. including the early Anthropocene hypothesis, see Ruddiman et al., 2011; Waters et al., 2018; Zalasiewicz et al., 2018), introduces a new phase, with landscape and habitat stability becoming highly random (still poorly evaluated) as a result of global climate perturbations induced by mankind (e.g. Ruddiman and Thomson, 2001; Crutzen, 2002; Steffen et al., 2011; Waters et al., 2016; Zalasiewicz et al., 2018; see also Lambert et al., 2018 for an illustration involving estuaries in north-western France).

It becomes essential, then, to test to what extent the dynamics of human populations are constrained by climatic hazards, with their direct and indirect environmental corollaries. This question requires a long-term (multi-millennial) perspective, which alone can provide access to time scales revealing environmental thresholds and shifts that potentially affected (and even constrained) populations. In this way, retrospective views are essential and make it possible to line up archaeological knowledge, often of a diachronic character, alongside the Earth's natural reference system. This is one key objective of palaeoclimatology, together with the extending of data beyond the brief time span of

instrumental records (and beyond biases arising from modern-day anthropogenic effects). Another crucial objective is to draw up an inventory of past climatic situations, analogous to or contrasting with the current period, to provide a clearer understanding of natural climate sensitivity and its natural envelopes of variability from local to global scales (e.g. Rehfeld et al., 2018; Penaud et al., 2020).

On millennial scales, the dominant natural climatic modes still have to be detected: their characterization being critical to improving the predictive capacities of climate models (Liu et al., 2014; Hernandez et al., 2020). This endeavour has recently led to major works on the compilation and inter-comparison of climate series targeting the recent Holocene period in particular, i.e. the last two millennia (Kaufman et al., 2020; PAGES 2k Network, 2013; McGregor et al., 2015). Solar and volcanic activity (historical period) have been demonstrated to be key drivers, as has anthropogenic activity for the most recent periods (e.g. Ruddiman et al., 2011, 2016). The Holocene has long been viewed as a stable period compared to the last glacial (e.g. Rehfeld et al., 2018) and only a few notable cold episodes due to drift-ice advection events mainly from the Labrador Sea and Arctic Ocean have been identified as significant (known as Bond events, Bond et al., 1997, 2001, or "Rapid Climate Change" events (RCCs) of Mayewski et al., 2004, including the 8.2 ka cal BP event; see also Fernane et al., 2015; Penaud et al., 2020 for a synthesis for France). Studies conducted throughout northern Europe reveal periods of severe storms during the Holocene (e.g. Goslin et al., 2018a and b, 2019), and such events, which are especially well highlighted in Brittany (e.g. Van Vliet Lanoë et al., 2014), have mostly been linked with cold periods, even locally in south-west France where our study is focused (Clarke et al., 2002; Bertran et al., 2020; Bertran and Fouéré, 2020). Storm frequency has also been related to one of the most significant modes of climate variability in the northern hemisphere, the North Atlantic Oscillation (NAO), and to AMOC (Atlantic Meridional Overturning Circulation) dynamics (e.g. Sorrel et al., 2012; Goslin et al., 2018a and b, 2019; Hernandez et al.,

92 2020). However, the processes that govern these infra-orbital climatic instabilities are still subject to
93 discussion.
94 The present work similarly aims to detect and account for Holocene palaeoenvironmental changes,
95 with special consideration of scaling effects in those processes, ranging from local to synoptic views.
96 The paper takes advantage of a dual approach combining climate history and human history. This is
97 done by way of two overlapping lines of study, with the twofold exploitation of: (1) a coastal
98 sedimentary accumulation feature recording the presence of human activity from Mesolithic and
99 Neolithic times (e.g. Verdin et al., 2019a), in addition to high-resolution facies variability, that is
100 directly comparable with (2) reference archives from which a tentative reconstruction of Holocene
101 climatic modes can be made (especially work derived from the ANR HAMOC, see
102 acknowledgments).
103 The main events consistent with records for the proximal Bay of Biscay will be highlighted here
104 together with the extent to which they are in phase with indices of climatic oscillations detected on a
105 broader spatial scale.
106
107

108 ## 2. The exceptional Lède du Gurp record

109 The Lède du Gurp (LDG) site is an archaeological site buried under modern dunes along the western
110 shore of the north Medoc peninsula, on the administrative boundary of the towns of Soulac-sur-Mer
111 and Grayan-et-l'Hôpital (Figure 1). This site is currently subject to chronic erosion, typical of
112 Aquitaine coastal zones associated with a river mouth (Gironde estuary). The area has been studied
113 by archaeologists since the mid-20th century and high-resolution excavations were conducted
114 between 1972 and 1999, especially on the topmost layers dated from the Iron Age (Hallstatt
115 civilization) where evidence of a local industry (and even habitats) dedicated to salt production was

116 reported (e.g. Frugier, 1972, 1975; Roussot-Larroque and Villes, 1988). The archaeological site
117 probably covered as much as half a hectare (i.e. 5000 m^2) judging by the local rate of erosion (close
118 to 10 m/year, e.g. Aubié and Tastet, 2000) and the discoveries of human artefacts in the vicinity,
119 reported both in the intertidal zone and in nearby depressions within the modern supratidal dunes. In
120 2014 drastic erosion of the shore and the dune front left a circular residual buttress (relief inversion,
121 Figure 1c) some 15 m in diameter and about 4 m high, made up of an accumulation of peaty and
122 sandy mud (see Faye et al., 2019; Verdin et al., 2019a). Rescue excavations were undertaken in
123 October 2014 revealing an extraordinary archaeological content (Verdin et al., 2016, 2019a and b)
124 and allowing the recovery from the buttress of continuous vertical sedimentary sequences up to 3 m
125 in length. A large set of analyses was applied to the recovered sequences (see Faye et al., 2019 for the
126 whole array of acquired data and detailed description of the studied records) and revealed an
127 uninterrupted high-resolution record for the last 10 ka. The present work follows on from Faye et al.,
128 2019 and Verdin et al., 2019a, which presented in detail the geology and sedimentology of the LDG
129 site, and the stratigraphic and archaeological contexts, respectively. Additional radiocarbon datings
130 (Table 1) enable us to focus here on climate-related proxies (especially those of palynological
131 analyses and high-resolution X-ray fluorescence - XRF scanning for major element quantification) in
132 a robust chronostratigraphic framework (9–3 ka interval). The sedimentological context of the
133 residual buttress from which the sequences were retrieved is linked to a circular depression within
134 blue-grey clayey-sands (completely eroded in 2014), infilled with argillaceous (and some
135 arenaceous) peaty deposits to a depth of approximately 4 m, since 10.5 ka BP at least; this age being
136 the oldest obtained by drilling (labelled SC1 in Table 1) in the deeper part of the peaty clays before
137 their transition with the blue-grey sandy deposits surrounding and delimiting the peaty depression. It
138 is assumed the depression was formed in an inner estuarine marshland in a context of karstic erosion,
139 possibly forced by thermokarstic processes (see Faye et al., 2019 for a discussion of this hypothesis)
140 considering the age obtained for the basal section of the record.

141 This new high-resolution Holocene record makes it possible to document long- and short-term
142 palaeoenvironmental variations both locally and globally. In line with ongoing efforts by the
143 palaeoclimatology community to compile past climatological records from diverse settings (e.g.
144 Kauffman et al., 2020, see also for instance existing sequences within the framework of the European
145 pollen database, http://www.europeanpollendatabase.net/fpd-epd/bibli.do, or work compiled for the
146 last 2 ka: https://pastglobalchanges.org/science/wg/2k-network/scientific-goals), it may provide key
147 signals in a context of growing human influence throughout the last millennia, helping us to identify
148 natural and anthropogenic shifts that have driven changes in European landscapes.
149
150 **2.1. Methods**
151 The detailed sampling protocol in the field together with the details of laboratory analyses of the
152 sediment sequences LDG-G3 (-1.154745; 45.466222) and LDG-G4 (-1.154759; 45.466085) are
153 described in Faye et al. (2019). Briefly, after the recovery of sections several metres in length
154 (continuous slab-composite sequences based on Nx25 cm long aluminium slides, with N=11 for
155 LDG-G3 and N=9 for LDG-G4, respectively) from the bottom to the top of the buttress, non-
156 destructive (scanning, using classic and X-ray imaging, coupled with spectrocolorimetry and XRF
157 measurements) and destructive analyses were conducted at the EPOC laboratory (see Faye et al.,
158 2019). The latter comprised a complete sub-sampling of sediment sections at 1 cm intervals for
159 sieving (at 150 µm) of the samples in order to determine their lithology and biostratigraphy (with
160 grain-size analyses of raw samples, visual description of the sandy > 150 µm fraction, radiocarbon
161 datings – Table 1, and palynological processing and analyses for the < 150 µm fraction).
162 The results presented and discussed here were compiled by age after the construction of independent
163 age scales for the LDG-G3 and LDG-G4 sequences (hereafter referred to as G3 and G4) based on 4
164 and 5 datings for each, respectively. Those chronological markers presented no reversals along the
165 sequences (Figure 2) and the global stratigraphy of the site covered at least the last 10.5 ka cal BP.

166 This was confirmed by separate datings obtained on organic archaeological remains (see Verdin et
167 al., 2019a and Faye et al., 2019). Age models were obtained by a polynomial regression (order 3). To
168 validate this approach, age-depth models were also produced with the "Undatable" age-depth
169 modelling routine (Lougheed and Obrochta, 2019) providing very similar age-model equations (not
170 used in the following, but their 1σ and 2 σ envelopes are plotted in Figure 2 to illustrate the
171 coherence of the methods).
172 Statistical analyses were conducted on XRF ratios (variables being the element/SUM ratio, the most
173 common way to normalize raw XRF cps data, and equivalent to relative percentages) to validate the
174 interpretation of the elemental changes detected. Those analyses were performed with PAST software
175 (PAleontological Statistics, Hammer et al., 2001). Our multivariate analysis based on an ordination
176 method, principal component analysis (PCA), was supplemented by ternary plots also provided by
177 PAST tools to better understand the significance of the highest scores on the main components.
178 Holocene sea-surface hydrographic conditions from the proximal southern Bay of Biscay PP10-07
179 core, used here for a comparison with the LDG signals, were reproduced from earlier works by Mary
180 et al. (2017) and Eynaud et al. (2018). Reconstructed hydrographic data were derived from
181 planktonic foraminifera assemblages after the MAT1007 transfer functions developed at EPOC (see
182 Eynaud et al., 2018 for a review of this approach). For this article, past sea-surface salinities (SSS)
183 were added to sea-surface temperature (SST) information thanks to an update of the modern
184 hydrographical database (mainly after the World Ocean Atlas 2013;
185 https://www.nodc.noaa.gov/OC5/woa13/woa13data.html, see methods in de Vernal et al., 2020). This
186 update enabled us to robustly reconstruct SSS on the basis of planktonic foraminifera (Root mean
187 square error of prediction of 0.7 psu).
188
189 **2.2. Main results and interpretation perspectives of the recorded signals**

XRF data from the G3 and G4 sequences have been compared systematically (when data co-exist) as the parallel between them provides very important information as to whether the records are coherent and complete. Actually, because of the large number of human artifacts found within the buttress during excavation, including wattle-work structures of a metre or so in size (Verdin et al., 2019a, López-Romero et al., 2021), doubts have arisen about whether the stratigraphy is continuous. The G3 and G4 sequences retrieved were some 15 metres apart (Figure 1), at the southern and northern ends of the buttress, respectively. Figures 3 and 4 show that, whatever the elemental ratio or concentration considered (as seen with the ratios for Fe/SUM in Figure 3b, S/SUM in Figure 3h, and Ti/SUM in Figure 4f), few discrepancies are to be found between the records whether in depth (see Faye et al. 2019) or age (despite independently built age-models). This confirms that the LDG site stratigraphy obtained is not only robust but also that it was not impacted by past human activities, at least on its outer edges.

By means of the diverse proxies, the studied records provide a detailed account of local environmental changes (linked or not to human influences, see Faye et al., 2019 for further details on the sedimentology of the sequences analysed) over the time window from 9 to 3 millennia (ka) before the present (cal BP, i.e. ~7 to 1 ka cal BCE/CE). As underlined in Figures 3 and 4, the most noticeable features encountered in those records are related to stepwise changes in most of the proxies. These changes reflect well-known environmental events within the Holocene and can be sequenced consistently with the climatic history of this period, with from the base to the top of the sequence:

– A first period of 3 millennia (from 9.4 to 7.1 ka cal BP) that records rapid but moderate amplitude changes in the proxies studied and so in the environmental contexts of the deposits. In the study area, that period was one of dense forest cover (Figure 3d) with predominantly deciduous *Quercus* (Figure 3j) and a moderate contribution of *Pinus* trees (Figure 3f). This part of the early Holocene (the

Greenlandian, Gibbard, 2018, also corresponding to the preboreal and boreal chronozones, Figure 4) still records significant climate changes mainly due to melt-water pulses associated with the retreat and melting of boreal ice-sheets (e.g. Elmore et al., 2015; van der Bilt et al., 2015). We have chosen to illustrate the regional expression of this decay in the declining volcanic activity in the Massif Central (Figure 4h) which may have caused lithospheric relaxation.

– A transitional period, between 7.1 and 6.1 ka cal BP, where all the proxies record radical shifts with marked excursions (Figure 3). None of the records depict similar values either before or after that period, and the changes are especially drastic for pollen assemblages (Figure 3d-e-f and 3j-k) and the K/SUM, S/SUM, Ca/SUM, Br/SUM ratios (Figure 3g-h-i and 3c). Two peaks in *Pinus* pollen bracket this short interval (Figure 3f). They are found along with a major decline in forest cover but they may also indicate strong winds (the preferential mode of dispersion of *Pinus* pollen grains) across the study area. This interval is also characterized by the largest values observed in the Fe/SUM record (Figure 3b) and by an excursion in the Br/Si signal in G3 (Figure 4e). Those observed changes are contemporaneous with mid-Holocene sea-level stabilization and precede the dip in insolation after 6 ka (e.g. Lorenz et al., 2006) and then the period known as the Neoglacial cooling in the northern hemisphere (Figure 4).

– Finally, the 6.1 to 3.4 ka cal BP period exhibits relatively flat records with rare excursions of the proxies from their background values, except between 5.4 and 4.8 ka cal BP, where moderate to high amplitude peaks are detected in granulometry (Figure 3a) and in the Fe/SUM, K/SUM (Figure 3b-g) and Br/Si signals of G3 especially (Figure 4e). The decline in forest cover is confirmed and attested by the corresponding expansion in grassland (Figure 3d-e-f-j-k). The period encompasses the Northgrippian-Meghalayan transition (Gibbard, 2018; Walker et al., 2019; Curran et al., 2019) and is marked locally by the onset of dune build-up along the Aquitanian coast, although dune migration and invasion peaked later (Tastet and Pontee, 1998; Clavé, 2001; Clarke et al., 2002; Stéphan et al.,

2019; Bertran et al., 2020; Bertran and Fouéré, 2020), during historical times (not covered by our records).

Apart from this distinct time division within the records compiled for the Holocene, the most significant result is that local changes detected in the XRF-derived data fit quite well, both in their pacing and amplitudes, with those relating to a hemispheric or even global climatic signature. These common detected trends argue for large scale processes imprinted within the records, despite numerous local geomorphological evolutions in the vicinity of the LDG site, that one can imagine to be factors of bias in its sedimentology, but which, visibly here, do not overprint or obliterate regional (i.e. the North Atlantic province) signals and global scale forcings. Figure 4 especially underlines the fit between LDG records and Holocene chronostratigraphic and climatological reference frameworks. These frameworks have been extensively supplemented over the last 20 years (see the number of existing records in the compilation in Kauffman et al., 2020) pointing out the strength of regionalism in the detected signals, and showing that climate is not the result of a single ruling component. Furthermore, uncertainties in those reconstructions are not failures in comprehending the system but rather proof of its extraordinary complexity. Local signals are a mixture of environmental interplay and the unravelling of the associated factors at play is critical to an understanding of changes in past ecosystems.

3. From a local to a global perspective

The LDG archaeological site thus extends our knowledge by providing an opportunity to test the synchronicity of well-known Holocene climatic and environmental events on France's south-west coast at a site that captured influences of natural ecosystem changes and growing anthropic pressure.

262 The reconstructed history may thus yield new information about the co-evolution of local natural
263 habitats and human trajectories within the framework of major climatic trends.
264
265 **3.1. Significance of the information recovered from the LDG archaeological site: What are**
266 **we recording?**
267 Sedimentary records integrate different physical and biogeochemical processes occurring on various
268 scales of time and space. Detecting climate events in such records is a complex matter and calls for
269 the local window of study to be opened up to broader contexts, to avoid misinterpretation or
270 misdetection in the environmental history. Here the perspective is thus drawn on the scale of the
271 Atlantic basin, which is known to concentrate various kinds of systemic response because of its key
272 role in the natural evolution of climate. Several records were selected to support our approach (Figure
273 4): they are distributed from pole to pole and selected so that events occurring during the Holocene
274 can be viewed against a regional or global background.
275 Local signatures and proxies reflect long-term climatic variations throughout the period under study.
276 This is especially true when comparing temperature signals, both on large geographical scales and for
277 more proximal systems (here SST of the southern Bay of Biscay). Our analyses show that the
278 K/SUM ratio seems to follow summer SST trends as reconstructed for the eastern tropical Atlantic
279 Ocean (Figure 4c and j). Similar coherence is observed for the Ti/SUM ratio, which fits neatly within
280 the envelope of global mean temperature anomalies (as compiled by Marsicek et al., 2018, Figure 4f
281 versus 4m). The Mn/SUM and Br/Si ratios similarly track the long-term evolution of summer SSTs
282 as reconstructed for the Bay of Biscay with, especially, a very flat signal after 6 ka cal BP (Figure 4d
283 versus 4k and Figure 4e versus 4l). Between 9 and 3 ka cal BP, the AP/NAP (arboreal – *including*
284 *Pinus*/non arboreal pollen) ratio shows the same declining values towards the present as those of the
285 global concentration of atmospheric methane (Figure 4g versus 4n). This observation may relate to a
286 close connection between vegetation dynamics and the global methane budget (i.e. from Sánchez-

287 Goñi et al., 2008 to Beck et al., 2018). However, the question of the latitudinal position of methane
288 sources and related vegetation type contributions is still open, especially for the Holocene, and is
289 furthermore puzzling with regard to the "early anthropogenic hypothesis" (e.g. Ruddiman and
290 Thompson, 2001). There are signs of forest clearance at the LDG site as early as 7 ka (Figure 3d-e-f-
291 j-k). Unfortunately the LDG records do not yield data for the last 3 ka. Therefore our study does not
292 encompass the mid-to-late Holocene rise seen in methane concentrations and attributed to the land-
293 use changes and forest clearance concomitant with agricultural development (Tzedakis, 2010;
294 Ruddiman et al., 2016).
295 The LDG sequences reveal several short-lived events superimposed on this early to mid-Holocene
296 trend. Some of these events are directly reflected in the compiled reference records, while others
297 appear to be exclusively local. The early Holocene especially records larger amplitude fluctuations
298 with three short but prominent peaks (maximum of 150 years' duration) which are clearly visible in
299 the Zn/SUM ratio (Figure 4b) at 8.7, 8.3 and 8.1 ka cal BP. Those peaks reflect sudden SST changes
300 in the proximal Bay of Biscay (Figure 4k and 4l) with significant warmings in annual SST (up to
301 8 °C, Figure 4l) at 8.7 ka cal BP. The last two peaks bracket the well-known cold "8.2 ka event" of
302 the NGRIP stratotype (Figure 4i, Vinther et al., 2006; Rasmussen et al., 2006) related to the complete
303 disappearance of the Laurentian ice cap with the drainage of Lake Agassiz (e.g. Clark et al., 2001)
304 that ended the Greenlandian (Walker et al., 2019). This spiky and noisy signal, well expressed in the
305 Zn/SUM ratio (Figure 4b), continues with recurrent events every 2 to 3 centuries up to 6 ka and then
306 flattens. This flattening seems to mark nearly all the records and is also seen in the proximal Bay of
307 Biscay, with mean annual SSTs reaching stable modern values (close to 14 °C, Figure 4l). This
308 stability is also confirmed for regional summer SST anomalies (Figure 4k) at the distal Cape Verde
309 tropical site (de Menocal et al., 2000, Figure 4a), with anomalies remaining close to zero, suggesting
310 steady climatic conditions over the North-Eastern Atlantic. Two late events can, however, be pointed
311 out (especially seen in the Fe/SUM and K/SUM ratios): they occur at 5.4 and 4.8 ka respectively

312 (Figure 3b and g and 4c), in a warm context as inferred from the related temperature records, and are
313 well circumscribed within the LDG site (corresponding also to brief lows in CH_4 concentration)
314 where they delimit a sand deposition event as measured in G3 (Figure 3a).
315
316 The changes highlighted at the local LDG site thus illustrate the change in sediment facies (see also
317 Faye et al., 2019 for the interpretation of grain-size data in the LDG records), occurring consistently
318 with environmental change. But what is the genetic link between the proxies used and climate? Since
319 the generalization of XRF core scanning tools, many attempts have been made to identify the
320 significance of elements in diverse sedimentary contexts (see especially the compilations in Croudace
321 and Rothwell, 2015; Croudace et al., 2019; for the organic matrix at the LDG site, see also Longman
322 et al., 2019). The most significant ratios in the LDG record (as deduced from the PCA analysis of G3
323 and also seen in G4) include the Fe/SUM, Ca/SUM, K/SUM, Si/SUM and S/SUM ratios. All of these
324 display high scores (negative and positive) for the two first components, accounting for 96% of the
325 variance (Figure 5). Ternary plots were drawn in addition to identify the sedimentological
326 significance of key ratios (Figure 5b). However, as previously illustrated with Figures 3 and 4, other
327 ratios of low weight in the PCA (Zn/SUM, Mn/SUM, Ti/SUM and Br/Si) should not be ignored as
328 they also clearly reflect environmental changes. Classically, in siliciclastic sediments from the North
329 Atlantic region, Ti, K, Si and Fe abundances are related to terrigenous inputs while Ca, Sr, S and Br
330 are related rather to biogenic production (e.g. Richter et al., 2006; Rothwell and Croudace, 2015;
331 Mojtahid et al., 2019; Longman et al., 2017, 2019). Additionally, S is often used as a proxy for
332 oxygen depletion/anoxia (Rothwell and Croudace, 2015).
333 In a similar coastal context (mouth of the Rega Valley, Baltic Sea), Harff et al. (2011) interpret
334 Holocene lithological facies by PCA analysis also performed on XRF data, attributing high
335 concentrations of K and Ti to high terrestrial discharge, whereas low K and Ti are associated with
336 increasing pelagic deposition together with a potential imprint of aeolian dust inputs. This scheme is

337 of course basin-dependent and the drainage valley of the Gironde and its surrounding geological
338 formations are quite different, preventing us from making a similar direct interpretation for our study
339 site. It can be further complicated by the large amount of organic matter (peaty facies) in our record.
340 However, considering a very recent Holocene study conducted in similar peaty sediments, and
341 despite a highly specific environment, namely the Mohos volcanic crater (Eastern Carpathians,
342 Romania; Longman et al., 2017), K and Ti concentrations (supplemented by Si concentrations) were
343 again evoked as key elements for monitoring deposition fluctuations in dust sources (ranging from
344 proximal loessic provenances to distal Saharan ones). In a Danish coastal lake (Filso), closed by sand
345 dunes during the Holocene, Goslin et al. (2017, 2018a and b, 2019) identify Mn, Fe and S as opposed
346 to Si and K. They attribute this contrast to a sandy origin associated with a river source characterized
347 by high Mn, Fe and S contents, whereas beach and dune sands are identified by high Si and K values.
348 Again, this interpretation is specific to their study area, but it is comparable to observations made on
349 the basis of LDG-G3 data, except for Ti, which is very scarce in our record. This is also consistent
350 with the geochemical analyses documented at the scale of the Aquitaine basin in Sitzia et al. (2017)
351 for fossil aeolian deposits: with K and Si found in aeolian sands and Ti in their analysis bearing a
352 signature related to loess and the fine fraction of cover-sands. In the LDG-G3 record, K and Si
353 content are positively correlated on PC1 and PC2, forming one common pole. Mn and S exhibit
354 contrasting polarities, and are negatively correlated on PC1 and PC2 (Figure 5a). Fe is the most
355 abundant element with a high negative score on PC2 (whereas its score is moderately positive on
356 PC1, Figure 5a) and contrasts with Ca (with a high negative score on PC1). The (Si+K)/Fe ratio can
357 therefore be here used as a tracer of sand blows over the LDG site.
358 Fe is a redox-sensitive element; to ascertain its degree of mobility in our record, correlations can be
359 tested between what are considered to be immobile (Ti) and mobile (K) elements. Actually,
360 according to Rothwell and Croudace (2015), high correlation between Ti and Fe and between Ti and
361 K indicates "that the downcore distribution of those elements is mostly unaffected by post-

362 depositional mobilisation via groundwater leaching and/or organic activity". In G3, we obtained a
363 high correlation between Fe and Ti (R2: 0.9162) and between Ti and K (R2: 0.9347).
364 At the LDG site, other significant trends in elements, as identified in Figure 4, include: (1) Mn/SUM
365 and Br/Si match the low amplitude evolution of SST in the Bay of Biscay whereas K/Sum matches
366 changes from the tropical site ODP658; (2) Ti/SUM, although low, matches global mean temperature
367 anomalies. Those elements therefore point to a direct/indirect link with the North Hemisphere
368 climatic regimes that we examine further in the next section.
369
370 **3.2. Forcing at play and teleconnections on the pan-Atlantic scale during the Holocene**
371 In order to synthetize information yielded by the LDG records and integrate it into a genetic
372 perspective of environmental pressures at play, we compiled a final figure (Figure 6) comparing the
373 respective loadings on PC1 and 2 (and their related key elemental ratios and proxies in the LDG)
374 with reconstructions of various forcings over the period of interest. Those forcings are classified so as
375 to describe trends which reflect:
376 – a long term evolution, as seen with PC1 (Figure 6e), here compared with the emblematic SST
377 record from the Scotian margin (north-western subpolar Atlantic) after Sachs (2007, Figure 6k), used
378 in several compilations for Holocene climatic changes (Marcott et al., 2013; Marsiceck et al., 2018);
379 – sub-millennial variability imprinted in PC2 (Figure 6f) and here compared with the Atlantic
380 storminess record reconstructed from Danish records by Goslin et al. (2018a and b, Figure 6c), Arctic
381 glacier activity detected in the sensitive region of Svalbard after van der Bilt et al. (2015, Figure 6a),
382 and the proximal sea-surface conditions in the Bay of Biscay (Cap-breton canyon terrace record,
383 some 200 km from the LDG site, Eynaud et al., 2018, Figure 6i).
384 A striking correspondence between climate modulations over the Holocene is thus detectable for the
385 various sites in the compilation over both the short and the long term (despite the use of different
386 dating methods). This reinforces previously raised observations (also illustrated in Figures 3 and 4)

387 and demonstrates that the LDG site has recorded the combination of local and distal climatic shifts,
388 emphasizing the high degree of coupling and teleconnections driving environmental changes during
389 the Holocene around the North Atlantic Ocean.
390 Many modern-day modes of climatic variability (namely for our zone, the NAO, Atlantic
391 Multidecadal Variability/Oscillation: AMV/AMO, Northern Annular Modes: NAM also named the
392 Arctic Oscillation: AO) have already been evoked to explain Holocene variability. All infer a strong
393 coupling between the atmosphere and Atlantic Ocean dynamics (e.g. Curan et al., 2019; Hernández et
394 al., 2020) especially along the track of westerlies. Here, we illustrate this coupling by sea-surface
395 salinity (SSS) reconstructions for the southern Bay of Biscay (Figure 6i), those SSS values
396 remarkably reflecting the storminess index of Goslin et al. (2018a and b, Figure 6c), with high SSS
397 values corresponding to high storminess. The genetic link explaining this correspondence, intrinsic to
398 ocean/atmosphere couplings, lies also in teleconnections that are not easy to disentangle, and
399 potentially convergent and interrelated processes: wind tracks and stresses over the ocean, dynamics
400 of the North Atlantic gyres driving saline incursions in the Bay of Biscay (from the south and the
401 north as well potentially), precipitation changes over Europe, Mediterranean outflow (MOW)
402 modulations (e.g., Lozier and Stewart, 2008), all affecting the balance of modern-like modes (see the
403 recent article of Montoya Duque et al., 2021, trying to find a genetic link between midwinter
404 European climate and storm tracks).
405 The mid-Holocene transition marks a critical shift in the records, as is well expressed in PC1
406 especially, objectively related to the well-known cooling trend following the climatic optimum after
407 the stabilization of boreal glacier melting and of the sea-level rise to its modern level, but not only
408 that. In many western European records, climatic deteriorations then intensified. This corresponds
409 roughly to the onset of primary dune aggradation in the bas-Médoc which culminated between 5 and
410 2 ka BP with prominent migration phases during historical times (Tastet and Pontee, 1998; Bertran et
411 al., 2020; Bertran and Fouéré, 2021). The progressive influence of dune invasions and migrations

412 along the Aquitanian coast may be expressed throughout the LDG records. It is suggested that active
413 phases of dune building occurred during negative NAO-phases and in relation to the availability of
414 sedimentary material (Clavé, 2001; Clarke et al., 2002; Van Vliet Lanoë et al., 2014; Bertran and
415 Fouéré, 2021). It is worth noting that the mid-Holocene also corresponds to accelerated regression
416 (clearance?) of European forests (as recently underlined on a regional Atlantic scale by Penaud et al.,
417 2020 and also seen locally, Figure 3d-e-f-j-k, Figure 6d) and thus that dune aggradations may also be
418 related to biorhexistasy effects.
419 This mid-Holocene shift has been observed in many records on the basis of many different proxies
420 (both marine and terrestrial); mechanistically it was often related to geographical shifts in the NAO
421 centres or related modes (e.g. Mauri et al., 2014), but no consensus really exists to identify a rather
422 positive or negative NAO-like configuration after or before. Probably, the stabilization of ice-sheet
423 melting rates at that time, as a corollary to steady sea-levels and few changes in the altimetry of
424 residual boreal ice-sheets, may have promoted the onset of modern climatic modes coupling
425 atmospheric and oceanic dynamics in the North Atlantic province. However, the literature contains
426 too few reconstructions of NAO, AMO or AMOC variability for the mid-Holocene transition to
427 generalize a pattern regarding those modes.
428 The following sub-millennial changes are furthermore difficult to relate to natural climatic shifts
429 alone, as anthropogenic influences increased with the settlement of Neolithic populations
430 (synchronously thus with the mid-Holocene shift). The LDG record provides new evidence when
431 looking at the related PC2 proxies (bottom part of Figure 6: b, f, g, h). Actually, the striking
432 coevolution of those local proxies with Svalbard glacier advance indexes (van der Bilt et al., 2015,
433 Figure 6a) between 6 and 3 ka cal BP, argues for common drivers in both temperate and boreal
434 latitudes. Furthermore those drivers had to be capable of generating a rapid transfer of perturbations,
435 as the most abrupt ones detected occurred in less than a century. Four events are especially noticeable
436 regarding their synchronicity: at 5.4, 4.8, 4.2 (a well-known Holocene climatic event, e.g. Jalali et al.,

2019), and even at 3.3 ka, the termination of the G3 record being due to the recovery of a highly peaty facies preventing us from collecting an undisturbed sample from the topmost layers (see Faye et al., 2019). The centennial scale glacier advances reported by van der Bilt et al. (2015, Figure 6a) thus find direct counterparts (or vice-versa) in the sand-blowing regression (as seen in the (Si+K)/Fe ratio in Figure 6b) and thus conversely peat developments along the Aquitaine coasts. This suggests that for times when wetter conditions are recorded in Aquitaine, something which also seems to have coincided with the dynamics of storm events in Denmark (Figure 6c), small Svalbard glaciers were expanding. This clearly attests to the crucial role of warm humid advections in the climate balance of western Europe whatever the latitude considered. The mechanisms behind this convergence are thus not exclusively linked to an NAO-like pattern, which on the contrary decouples and contrasts mid-latitudes and polar-latitudes of Europe in terms of humidity conditions. Instead, we observe here a synchronicity which suggests and highlights a factor controlling temperature and humidity simultaneously along the eastern North Atlantic (possibly occurring under a relaxed north-hemispheric gradient). A "climatic valve", capable of nurturing small glaciers in Svalbard, storminess in Denmark and humidity in SW France, argues for multi-year-lasting dynamics and therefore an oceanic driver. The best candidate is modulation of the intensity of North Atlantic Drift (NAD) inflows towards the pole in the Nordic seas, i.e. in AMOC dynamics. The most recent literature suggests that AMOC was a key driver of Europe's Holocene climate, notably implying a strong reactivity with ice compartments (from marine-terminating glaciers, e.g. Curran et al., 2019, or sea-ice cover as well, e.g. Klein et al., 2014; Găinuşă-Bogdan et al., 2020). The causes of AMOC internal variability have still not been fully identified as they imply diverse interactions and feedbacks (purely physical – thermo-haline – or wind-related or both, but also probably linked to sporadic events such as volcanic forcing and to biospheric changes impacting the Earth's radiative budget), in a context of primary external insolation forcing. Despite those complex loops, one of the most probable, and often cited, processes is the recirculation of warm, (sub)tropically-sourced, Atlantic waters, along the

462 boundaries of the subtropical and subpolar gyres (Eynaud et al., 2018; Curran et al., 2019). The
463 eastward extension of the North Atlantic subpolar gyre, recently documented for the Holocene by
464 Colin et al. (2019) in the Rockall Trough, may have modulated this recirculation. It is worth noting
465 that the comparison of the millennial scale fluctuations identified in the composite record of cold-
466 water coral εNd by Colin et al. (2019) matches the (Si+K)/Fe ratio in G3 with especially high εNd
467 values recorded for low (Si+K)/Fe values. Interestingly those low values are also recorded for high
468 salinity values in the Bay of Biscay, something that we can relate to the modern observations of
469 Lozier and Stewart (2008) who attribute salinity anomalies in the eastern North Atlantic temperate
470 basins to a eastward expanded SPG blocking the northward MOW circulation up to the Nordic seas,
471 synchronously to a subpolar front moving eastward, a positive NAO index and strong westerlies.
472 Our study thus shows that even isolated records can capture climatic signals in a very sensitive
473 manner and are all very good candidates and proxies for directly or indirectly inferring the global
474 dynamics of climate. Past sequences usefully supplement modern observations and modelling
475 exercises as their indirect and integrated character may be an asset for picturing concepts on a
476 synoptic and comprehensive scale.
477
478 **3.3. Human population dynamics**
479 The transitions highlighted and events identified in the LDG sequences also correspond to major
480 shifts in European population dynamics and cultural developments during the Holocene as
481 summarized hereafter. The Neolithic period, marked by the expansion of farming and a radical shift
482 in belief systems, even if diachronous across Europe (due to a north-westward progression of
483 acculturation for central and northern Europe and a westward maritime-related progression for
484 Mediterranean Europe), coincided with the mid-Holocene, which is particularly well expressed here
485 as previously discussed (Figures 4 and 6). Beyond this major transition, the events at 5.4, 4.8 and 4.2
486 ka occurred at times of drastic changes, related especially to a succession of megadroughts in Eurasia

and Africa (e.g. Brooks, 2006; Weiss, 2016; Griffiths et al., 2020 and references therein). Those events encompassed the Late Neolithic/Chalcolithic periods and the transition to the Bronze Age, which are recognized as periods of increasing social complexity (Kristiansen and Larsson, 2005; Brooks, 2006; Milevski, 2013).

The 4.2 ka event has been chosen as the date of the transition between the Northgrippian and the Meghalayan (Walker et al., 2019). It is related to severe drought in the tropics and subtropics, that may have also affected European populations (e.g. Drysdale et al., 2006) as suggested by discoveries of groundwater collection systems and wells, contemporaneous with this episode and abandoned subsequently (see e.g. the "Motillas" Bronze Age horizon in central Spain, Mejías Moreno et al., 2014). At the LDG site and in its vicinity (e.g. the nearby site of Amélie beach), this period saw a significant increase in the number of Late Neolithic and Bronze Age remains, as past and present archaeological research has demonstrated (e.g. Roussot Laroque, 2007; López-Romero et al., 2021). Climate may have impacted local populations in several ways, but published evidence for the LDG site (Roussot Laroque, 1999; Roussot Laroque, 2007; Roussot Laroque, 2010) has documented occupation changes (gaps included) rather in relation to weather extremes such as drought and storminess. Several well-preserved wattle structures, probably related to the salt industry, have been found after 6 ka cal BP within the site (see pictures in Verdin et al., 2019a and López-Romero et al., 2021) indicating repeated exploitations of the area by Neolithic humans. During the Bronze Age, for which a very dense collection of anthropic artefacts has been collected, gaps in settlement were also reported to be synchronous with interruptions in farming pressure (Roussot Laroque, 2007).

This evidence suggests that during the part of the Holocene under study here, randomness due to sudden changes was superimposed on the long-term climatic trend initiated with deglaciation, and may have drastically impacted both the environment and human populations.

4. Conclusion

This study focused on a high-resolution archaeological record encompassing the early to late Holocene transition. On the basis of a palaeoenvironmental approach relying mostly on XRF and palynological (pollen) data, we found evidence for specific breaks in the sedimentological record that all find direct counterparts in the well-known pan-Atlantic climate shifts. The record under study reveals a long-term trend, classically echoing the evolution of Holocene insolation forcing, with superimposed short-term events bearing a more local signal related mainly to proximal North Atlantic Ocean dynamics. It highlights how western European environments (and therefore populations) were dependent upon the linearity of climate evolution. It suggests also that high-time-resolved records made up of both archaeological and environmental remains, even if local and at first sight "disturbed" by the presence of anthropic artefacts, are in fact, where they prove to be continuous, highly valuable sequences worth detailed study to better identify risk and resilience factors capable of affecting human societies.

5. Author contributions

All authors contributed to the published work. FE wrote the paper and conceptualized the study as part of the joint direction (funding acquisition and administration; investigation and methodological frameworks; analyses) of the LITAQ (conducted with FV) and HAMOC (conducted with CrC) projects. YM, EL-R, AP and CC were involved in both projects and contributed to the data produced and the related scientific discussions. CB was in charge of the analysis of pollen grain assemblages in G3.

6. Data availability

The data published in this article are available on request from FE.

7. Declaration of competing interest

The authors declare that they have no known competing financial interests or personal relationships that could have appeared to influence the work reported in this paper.

8. Acknowledgements

Financial support for this research was obtained thanks to the LITAQ project ("*Du Pléistocène à l'Anthropocène : connaître les mécanismes passés d'évolution des populations -végétales, animales, humaines- et des milieux pour prédire les réponses futures. L'exemple du LITtoral Aquitain*", supported by the French National Research Agency/ANR in the Programme Investissement d'Avenir framework - ANR-10-IDEX-03-02 within the Inter-clusters of Excellence COTE – ANR-10-LABX-45 and LaScArBx – ANR-10-LABX-52), and by the ANR HAMOC Project ("*Holocene North-Atlantic Gyres and Mediterranean Overturning Dynamic through Climate Changes*" - Grant ANR-13-BS06-0003). Fundings were also obtained for the analyses thanks to the INSU- EC2CO DRILL project FAST-LITAQ ("*Formations Argilo-Sableuses & Tourbes LITtorales AQuitaines : de leur intérêt dans l'évolution des falaises dunaires du Médoc"*) and to the INSU-TELLUS-ARTEMIS *2017* project "*Dynamique des peuplements humains et Climats : du Paléolithique à nos jours, mieux contraindre les périodes de ruptures culturelles*". The authors would like to thank all the other participants in these projects for their fruitful collaboration and discussion. We thank Isabelle Billy for XRF core-scanning measurements and Ludovic Deveaux for the pollen preparation.

9. References

Aubié, S., Tastet, J.P., 2000. Coastal erosion, processes and rates: an historical study of the Gironde coastline, southwestern France. Journal of Coastal Research 16, 756–767.

559 Beck, J., Bock, M., Schmitt, J., Seth, B., Blunier, T., Fischer, H., 2018. Bipolar carbon and hydrogen
560 isotope constraints on the Holocene methane budget. Biogeosciences 15, 7155–7175.
561 https://doi.org/10.5194/bg-15-7155-2018
562 Bertran, P., Andrieux, E., Bateman, M.D., Fuchs, M., Klinge, M., Marembert, F., 2020. Mapping and
563 chronology of coversands and dunes from the Aquitaine basin, southwest France. Aeolian
564 Research 47, 100628. https://doi.org/10.1016/j.aeolia.2020.100628
565 Bertran, P., Fouéré, P., 2020. The Holocene estuarine and coastal dune deposits of Soulac sur Mer
566 (Médoc peninsula, southwest France). Quaternaire 31/3: 231–248.
567 https://doi.org/10.4000/quaternaire.14277
568 Bertrand, F., Verdin, F., Eynaud, F., Arnaud-Fassetta, G., Stéphan, P., Costa, S., Suanez, S., 2019.
569 Settlement potential and constraints on the lower Médoc coastline: results of the Litaq project
570 and considerations on coastal palaeo-risks in the protohistoric periods. Quaternaire 30 (1), 97-
571 111. https://doi.org/10.4000/quaternaire.11228
572 Bond, G., Showers, W., Cheseby, M., Lotti, R., Almasi, P., de Menocal, P., Priore, P., Cullen, H.,
573 Hajdas, I., Bonani, G., 1997. A pervasive millennial-scale cycle in the North Atlantic Holocene
574 and glacial climates. Science 278, 1257-1266.
575 Bond, G., Kromer, B., Beer, J., Muscheler, R., Evans, M.N., Showers, W., Hoffmann, S., Lotti-Bond,
576 R., Hajdas, I., Bonani, G., 2001. Persistent solar influence on North Atlantic climate during the
577 Holocene. Science 294, 2130-2136. https://doi.org/10.1126/science.1065680
578 Brooks, N., 2006. Cultural responses to aridity in the Middle Holocene and increased social
579 complexity. Quaternary International 151, 29–49. https://doi.org/10.1016/j.quaint.2006.01.013
580 Clark, P.U., 2001. Freshwater Forcing of Abrupt Climate Change During the Last Glaciation. Science
581 293, 283-287. https://doi.org/10.1126/science.1062517
582 Clarke, M., Rendell, H., Tastet, J.-P., Clave, B., Masse, L., 2002. Late-Holocene sand invasion and
583 North Atlantic storminess along the Aquitaine Coast, southwest France. The Holocene 12, 231-
584 238. https://doi.org/10.1191/0959683602hl539rr
585 Clavé, B., 2001. Evolution de paléo-environnements côtiers à l'Holocène : exemple de l'Aquitaine
586 septentrionale. PhD thesis Bordeaux 1 University. 316 pp
587 Colin, C., Tisnérat-Laborde, N., Mienis, F., Collart, T., Pons-Branchu, E., Dubois-Dauphin, Q.,
588 Frank, N., Dapoigny, A., Ayache, M., Swingedouw, D., Dutay, J.-C., Eynaud, F., Debret, M.,
589 Blamart, D., Douville, E., 2019. Millennial-scale variations of the Holocene North Atlantic mid-
590 depth gyre inferred from radiocarbon and neodymium isotopes in cold water corals. Quaternary
591 Sc. Rev. 211, 93–106. https://doi.org/10.1016/j.quascirev.2019.03.011
592 Croudace, I.W., Rothwell, R.G. (Eds.), 2015. Micro-XRF studies of sediment cores. applications of a
593 non-destructive tool for the environmental sciences, Developments in paleoenvironmental
594 research 17. Springer, Dordrecht. https://doi.org/10.1007/978-94-017-9849-5
595 Croudace, I.W., Löwemark L., Tjallingii R., Zolitschka B., 2019. Current perspectives on the
596 capabilities of high resolution XRF core scanners. Quaternary International 514: 5-15.
597 https://doi.org/10.1016/j.quaint.2019.04.002
598 Crutzen, P.J., 2002. The "anthropocene." J Phys. IV France, EDP Sciences, Les Ulis 12.
599 https://doi.org/lO.10511jp4:20020447
600 Curran, M.J., Rosenthal, Y., Wright, J.D., Morley, A., 2019. Atmospheric response to mid-Holocene
601 warming in the northeastern Atlantic: Implications for future storminess in the Ireland/UK
602 region. Quaternary Sc. Rev. 225, 106004. https://doi.org/10.1016/j.quascirev.2019.106004
603 deMenocal, P., Ortiz, J., Guilderson, T., Sarnthein, M., 2000. Coherent high- and low-latitude climate
604 variability during the holocene warm period. Science 288, 2198–2202.
605 deMenocal, P.B., 2001. Cultural Responses to Climate Change During the Late Holocene. Science
606 292, 667–673. https://doi.org/10.1126/science.1059827
607 de Vernal, A., Radi, T., Zaragosi, S., Van Nieuwenhove, N., Rochon, A., Allan, E., De Schepper, S.,
608 Eynaud, F., Head, M.J., Limoges, A., Londeix, L., Marret, F., Matthiessen, J., Penaud, A.,

Pospelova, V., Price, A., Richerol, T., 2020. Distribution of common modern dinoflagellate cyst taxa in surface sediments of the Northern Hemisphere in relation to environmental parameters: The new n=1968 database. Marine Micropaleontology 159, 101796. https://doi.org/10.1016/j.marmicro.2019.101796

Drysdale, R., Zanchetta, G., Hellstrom, J., Maas, R., Fallick, A., Pickett, M., Cartwright, I., Piccini, L., 2006. Late Holocene drought responsible for the collapse of Old World civilizations is recorded in an Italian cave flowstone. Geology 34 (2), 101-104. https://doi.org/10.1130/G22103.1

Elmore, A.C., Wright, J.D., Southon, J., 2015. Continued meltwater influence on North Atlantic Deep Water instabilities during the early Holocene. Marine Geology 360, 17-24. http://dx.doi.org/10.1016/j.margeo.2014.11.015

Eynaud, F., Mary, Y., Zumaque, J., Wary, M., Gasparotto, M.-C., Swingedouw, D., Colin, C., 2018. Compiling multiproxy quantitative hydrographic data from Holocene marine archives in the North Atlantic: A way to decipher oceanic and climatic dynamics and natural modes? Global and Planetary Change 170, 48–61. https://doi.org/10.1016/j.gloplacha.2018.07.017

Faye, S., Eynaud, F., Bosq, M., Lambert, C., Verdin, F., Vequaud, P., Lodyga, O., Dériennic, H., Lebleu, P., Bujan, S., Billy, I., Martin, B., Roussot-Larroque(†), J., 2019. Holocene palaeoenvironmental evolution of the Médoc peninsula (SW France): insights from the sedimentological study of the "Lède du Gurp" archaeological site. Quaternaire 30 (1), 31-46. https://doi.org/10.4000/quaternaire.11164

Fernane, A., Penaud, A., Gandouin, E., Goslin, J., Van Vliet-Lanoë, B., Vidal, M., 2015. Climate variability and storm impacts as major drivers for human coastal marsh withdrawal over the Neolithic period (Southern Brittany, NW France). Palaeogeography, Palaeoclimatology, Palaeoecology 435, 136–144. https://doi.org/10.1016/j.palaeo.2015.05.029

Frugier, G., 1972. Sauvetage archéologique à Grayan (Gironde). Juillet -Aout 1972.

Frugier, G., 1975. Sondage archéologique de "la Lède du Gurp" Commune de Grayan (Gironde).

Găinuşă-Bogdan, A., Swingedouw, D., Yiou, P., Cattiaux, J., Codron, F., Michel, S., 2020. AMOC and summer sea ice as key drivers of the spread in mid-holocene winter temperature patterns over Europe in PMIP3 models. Global and Planetary Change 184, 103055. https://doi.org/10.1016/j.gloplacha.2019.103055

Gibbard, 2018. Formal subdivision of the Holocene Series/Epoch. https://www.qpg.geog.cam.ac.uk/news/formalsubdivisionoftheholoceneseriesgeogr18.pdf

Goslin, J., Clemmensen, L.B., 2017. Proxy records of Holocene storm events in coastal barrier systems: Storm-wave induced markers. Quaternary Sci. Rev. 174, 80–119. http://dx.doi.org/10.1016/j.quascirev.2017.08.026

Goslin, J., Fruergaard M., Sander L., Gałka M., Menviel L., Monkenbusch J., Thibault N., Clemmensen L. B., 2018a. Holocene Centennial to Millennial Shifts in North-Atlantic Storminess and Ocean Dynamics. Sci. Rep. 8, 12778. https://doi.org/10.1038/s41598-018-29949-8.

Goslin, J., Fruergaard, M., Sander, L., Galka, M., Menviel, L., Mokenbusch, J., Thibaut, N., Clemmensen, L.B., 2018b. Corrigendum version. Holocene centennial to millennial shifts in North-Atlantic storminess and ocean dynamics. Sci. Rep. 8, 12778.

Goslin, J., Gałka M., Sander L., Fruergaard M., Mokenbusch J., Thibault N., Clemmensen L. B., 2019. Decadal Variability of North-Eastern Atlantic Storminess at the Mid-Holocene: New Inferences from a Record of Wind-Blown Sand, Western Denmark. Global and Planetary Change 180, 16-32. https://doi.org/10.1016/j.gloplacha.2019.05.010.

Griffiths, M.L., Johnson, K.R., Pausata, F.S.R., White, J.C., Henderson, G.M., Wood, C.T., Yang, H., Ersek, V., Conrad, C., Sekhon, N., 2020. End of Green Sahara amplified mid- to late Holocene megadroughts in mainland Southeast Asia. Nature Com. 11, 4204. https://doi.org/10.1038/s41467-020-17927-6

Hammer, Ø., Harper, D.A.T., and P. D. Ryan, 2001. PAST: Paleontological Statistics Software Package for Education and Data Analysis. Palaeontologia Electronica 4(1): 9 pp.

Harff J., Endler R., Emelyanov E., Kotov S., Leipe T., Moros M., Olea R., Tomczak M., Witkowski A., 2011. Late Quaternary climate variations reflected in Baltic Sea sediments. In: Harff J, Björck S, Hoth P (eds) The Baltic Sea Basin, vol. 3, pp 99-132. https://doi:10.1007/978-3-642–17220-5_5

Hernández, A., Martin-Puertas, C., Moffa-Sánchez, P., Moreno-Chamarro, E., Ortega, P., Blockley, S., Cobb, K.M., Comas-Bru, L., Giralt, S., Goosse, H., Luterbacher, J., Martrat, B., Muscheler, R., Parnell, A., Pla-Rabes, S., Sjolte, J., Scaife, A.A., Swingedouw, D., Wise, E., Xu, G., 2020. Modes of climate variability: Synthesis and review of proxy-based reconstructions through the Holocene. Earth-Science Rev. 209, 103286. https://doi.org/10.1016/j.earscirev.2020.103286

Jalali, B., Sicre, M.-A., Azuara, J., Pellichero, V., Combourieu-Nebout, N., 2019. Influence of the North Atlantic subpolar gyre circulation on the 4.2 ka BP event. Clim. Past 15, 701–711, https://doi.org/10.5194/cp-15-701-2019

Jansen, E., Bjorklund, K.R., 1985. Surface ocean circulation in the Norwegian Sea 15,000 B.P. to present. Boreas 14, 243–257.

Kaufman, D., McKay, N., Routson, C., Erb, M., Davis, B., Heiri, O., Jaccard, S., Tierney, J., Dätwyler, C., Axford, Y., Brussel, T., Cartapanis, O., Chase, B., Dawson, A., de Vernal, A., Engels, S., Jonkers, L., Marsicek, J., Moffa-Sánchez, P., Morrill, C., Orsi, A., Rehfeld, K., Saunders, K., Sommer, P.S., Thomas, E., Tonello, M., Tóth, M., Vachula, R., Andreev, A., Bertrand, S., Biskaborn, B., Bringué, M., Brooks, S., Caniupán, M., Chevalier, M., Cwynar, L., Emile-Geay, J., Fegyveresi, J., Feurdean, A., Finsinger, W., Fortin, M.-C., Foster, L., Fox, M., Gajewski, K., Grosjean, M., Hausmann, S., Heinrichs, M., Holmes, N., Ilyashuk, B., Ilyashuk, E., Juggins, S., Khider, D., Koinig, K., Langdon, P., Larocque-Tobler, I., Li, J., Lotter, A., Luoto, T., Mackay, A., Magyari, E., Malevich, S., Mark, B., Massaferro, J., Montade, V., Nazarova, L., Novenko, E., Pařil, P., Pearson, E., Peros, M., Pienitz, R., Płóciennik, M., Porinchu, D., Potito, A., Rees, A., Reinemann, S., Roberts, S., Rolland, N., Salonen, S., Self, A., Seppä, H., Shala, S., St-Jacques, J.-M., Stenni, B., Syrykh, L., Tarrats, P., Taylor, K., van den Bos, V., Velle, G., Wahl, E., Walker, I., Wilmshurst, J., Zhang, E., Zhilich, S., 2020. A global database of Holocene paleotemperature records. Sci. Data 7, 115. https://doi.org/10.1038/s41597-020-0445-3

Klein, F., Goosse, H., Mairesse, A., de Vernal, A., 2014. Model–data comparison and data assimilation of mid-Holocene Arctic sea ice concentration. Clim. Past 10, 1145–1163. https://doi.org/10.5194/cp-10-1145-2014

Kristiansen, K., Larsson, T.B., 2005. The Rise of Bronze Age Society. Travels, Transmissions and Transformations. Cambridge: Cambridge University Press.

Lambert, C., Penaud, A., Vidal, M., Klouch, K., Gregoire, G., Ehrhold, A., Eynaud, F., Schmidt, S., Ragueneau, O., Siano, R., 2018. Human-induced river runoff overlapping natural climate variability over the last 150 years: Palynological evidence (Bay of Brest, NW France). Global and Planetary Change 160, 109-122. https://doi.org/10.1016/j.gloplacha.2017.11.004

Liu, Z., Zhu, J., Rosenthal, Y., Zhang, X., Otto-Bliesner, B.L., Timmermann, A., Smith, R.S., Lohmann, G., Zheng, W., Elison Timm, O., 2014. The Holocene temperature conundrum. PNAS 111, E3501-E3505. https://doi.org/10.1073/pnas.1407229111

Longman, J., Veres, D., Ersek, V., Salzmann, U., Hubay, K., Bormann, M., Wennrich, V., Schäbitz, F., 2017. Periodic input of dust over the Eastern Carpathians during the Holocene linked with Saharan desertification and human impact. Clim. Past 13, 897–917. https://doi.org/10.5194/cp-13-897-2017

Longman, J., Veres, D., Wennrich, V., 2019. Utilisation of XRF core scanning on peat and other highly organic sediments. Quaternary International 514, 85–96. https://doi.org/10.1016/j.quaint.2018.10.015

López-Romero, E., Verdin, F., Eynaud, F., Culioli, C., Hoffmann, A., Huchet, J.-B., Rollin, J., Stéphan, P., 2021. Human settlement and landscape dynamics on the coastline south of the Gironde estuary (SW France): A multi-proxy approach. The Journal of Island and Coastal Archaeology. https://doi.org/10.1080/15564894.2021.1880505

Lorenz, S.J., Kim, J.-H., Rimbu, N., Schneider, R.R., Lohmann, G., 2006. Orbitally driven insolation forcing on Holocene climate trends: Evidence from alkenone data and climate modeling. Paleoceanography 21, PA1002, https://doi.org/10.1029/2005PA001152

Lougheed, B. C., Obrochta, S. P., 2019. A rapid, deterministic age-depth modeling routine for geological sequences with inherent depth uncertainty. Paleoceanography and Paleoclimatology, 34, 122-133. https://doi.org/10.1029/2018PA003457

Lozier, M.S., Stewart, N.M., 2008. On the Temporally Varying Northward Penetration of Mediterranean Overflow Water and Eastward Penetration of Labrador Sea Water. Journal of Physical Oceanography 38, 2097–2103. https://doi.org/10.1175/2008JPO3908.1

Marcott, S.A., Shakun, J.D., Clark, P.U., Mix, A.C., 2013. A Reconstruction of Regional and Global Temperature for the Past 11,300 Years. Science 339, 1198-1201. https://doi.org/10.1126/science.1228026

Marsicek, J., Shuman, B.N., Bartlein, P.J., Shafer, S.L., Brewer, S., 2018. Reconciling divergent trends and millennial variations in Holocene temperatures. Nature 554, 92-96. https://doi.org/10.1038/nature25464

Mary, Y., Eynaud, F., Colin, C., Rossignol, L., Brocheray, S., Mojtahid, M., Garcia, J., Peral, M., Howa, H., Zaragosi, S., Cremer, M., 2017. Changes in Holocene meridional circulation and poleward Atlantic flow: the Bay of Biscay as a nodal point. Climate of the Past 13, 201-216. https://doi.org/10.5194/cp-13-201-2017

Mauri, A., Davis, B.A.S., Collins, P.M., Kaplan, J.O., 2014. The influence of atmospheric circulation on the mid-Holocene climate of Europe: a data–model comparison. Clim. Past 10, 1925-1938. https://doi.org/10.5194/cp-10-1925-2014

Mayewski, P.A., Rohling, E.E., Stager, J.C., Meeker, L.D., Meyerson, E.A., Gasse, F., van Kreveld, S., Holmgren, K., Lee-Thorp, J., Rosqvist, G., Rack, F., Staubwasser, M., Schneider, R.R., Steig, E.J., 2004. Holocene climate variability. Quaternary Research 62, 243– 255.

McGregor, H.V., Evans, M.N., Goosse, H., Leduc, G., Martrat, B., Addison, J.A., Mortyn, P.G., Oppo, D.W., Seidenkrantz, M.-S., Sicre, M.-A., Phipps, S.J., Selvaraj, K., Thirumalai, K., Filipsson, H.L., Ersek, V., 2015. Robust global ocean cooling trend for the pre-industrial Common Era. Nature Geoscience 8, 671–677. https://doi.org/10.1038/ngeo2510

Mejías Moreno, M., Benítez de Lugo, L., del Pozo Tejado, J., Moraleda Sierra, J. 2014. Los primeros aprovechamientos de aguas subterráneas en la Península Ibérica. Las motillas de Daimiel en la Edad del Bronce de La Mancha. Boletín geológico y minero 125 (4), 455-474.

Miallier, D., Pilleyre, T., Sanzelle, S., Boivin, P., Lanos, P., 2012. Revised chronology of the youngest volcanoes of the chaîne des puys (french Massif central). Quaternaire 23 (4), 283-290. https://doi.org/10.4000/quaternaire.6367

Milevski, I., 2013. The Transition from the Chalcolithic to the Early Bronze Age of the Southern Levant in socioeconomic context. In: Paléorient 39 (1). The Transition Late Chalcolithic to Early Bronze Age in the Southern Levant. Paléorient 39(1), 193-208. https://doi.10.3406/paleo.2013.5495

Mojtahid, M., Durand, M., Coste, P.-O., Toucanne, S., Howa, H., Nizou, J., Eynaud, F., Penaud, A., 2019. Millennial-scale Holocene hydrological changes in the northeast Atlantic: New insights from "La Grande Vasière" mid-shelf mud belt. The Holocene 29, 467–480. https://doi.org/10.1177/0959683618816478

Montoya Duque, E., Lunkeit, F., Blender, R., 2021. North Atlantic midwinter storm track suppression and the European weather response in ERA5 reanalysis. Theoretical and Applied Climatology. https://doi.org/10.1007/s00704-021-03517-z

PAGES 2k Consortium, 2013. Continental-scale temperature variability during the past two millennia. Nature Geoscience 6, 339–346. https://doi.org/10.1038/ngeo1797

Penaud, A., Ganne, A., Eynaud, F., Lambert, C., Coste, P.O., Herlédan, M., Vidal, M., Goslin, J., Stéphan, P., Charria, G., Pailler, Y., Durand, M., Zumaque, J., Mojtahid, M., 2020. Oceanic versus continental influences over the last 7 kyrs from a mid-shelf record in the northern Bay of Biscay (NE Atlantic). Quaternary Sc. Rev. 229, 106135. https://doi.org/10.1016/j.quascirev.2019.106135

Rasmussen, S.O., Andersen, K.K., Svensson, A.M., Steffensen, J.P., Vinther, B.M., Clausen, H.B., Siggaard-Andersen, M.-L., Johnsen, S.J., Larsen, L.B., Dahl-Jensen, D., Bigler, M., Röthlisberger, R., Fischer, H., Goto-Azuma, K., Hansson, M.E., Ruth, U., 2006. A new Greenland ice core chronology for the last glacial termination. J. Geophys. Res. 111, D06102. https://doi.org/10.1029/2005JD006079

Rehfeld, K., Münch, T., Ho, S.L., Laepple, T., 2018. Global patterns of declining temperature variability from the Last Glacial Maximum to the Holocene. Nature 554, 356–359. https://doi.org/10.1038/nature25454

Richter, T.O., Van Der Gaast, S., Koster, B., Vaars, A., Gieles, R., de Stigter, H.C., de Haas, H., Van Weering, T.C.E., 2006. The Avaatech XRF Core Scanner: technical description and applications to NE Atlantic sediments., in: Rothwell, R.G. (Ed.), New Techniques in Sediment Core Analysis. Geological Society Special Publications, London, pp. 39–50.

Rothwell and Croudace, 2015. Twenty Years of XRF Core Scanning Marine Sediments: What Do Geochemical Proxies Tell Us? Part I - Marine Studies: Chapter 2, in: I. W. Croudace and R. G. Rothwell (Eds), Micro-XRF Studies of Sediment Cores Applications of a non-destructive Tool for the Environmental Sciences, Developments in Paleoenvironmental Research 17, https://doi.org/10.1007/978-94-017-9849-5

Roussot-Larroque, J., Villes, A., 1988. Fouilles pré- et protohistoriques à La Lède du Gurp (Grayan-et L'Hôpital, Gironde). Revue Archéologique de Bordeaux Tome lXXlX.

Roussot-Larroque, J., 1999. Bronze moyen et final autour de l'estuaire de la Gironde, in: Actes Des Congrès Internationaux Des Sociétés Historiques et Scientifique, Systèmes Fluviaux. Presented at the 124eme, Nantes, pp. 253–271.

Roussot-Larroque, J., 2007. Emprises et déprises agricoles en médoc durant l'âge du bronze 9. In : H. Richard, M. Magny, C. Mordant dir., Environnements et cultures à l'âge du Bronze en Europe occidentale. Actes des Congrès nationaux des sociétés historiques et scientifiques, 129", Besançon, 2004. Paris, CTHS, p. 285-293 (Documents préhistoriques, n° 21).

Roussot-Larroque, J., 2010. Du Mésolithique au Néolithique ancien. Transitions ou rupture ?, in: De Néandertal à l'Homme Moderne. L'Aquitaine Préhistorique : Vingt Ans de Découvertes (1990-2010). Vincent MISTROT (coord.). Editions Confluences.

Ruddiman, W.F., Thomson, J.S., 2001. The case for human causes of increased atmospheric CH4 over the last 5000 years. Quaternary Sc. Rev. 20, 1769-1777. https://doi.org/10.1016/S0277-3791(01)00067-1

Ruddiman, W.F., Crucifix, M.C., Oldfield, F.A., 2011. Introduction to the early-Anthropocene Special Issue. The Holocene 21, 713–713. https://doi.org/10.1177/0959683611398053

Ruddiman, W.F., Kutzbach, J.E., Vavrus, S.J., 2011. Can natural or anthropogenic explanations of late-Holocene CO2 and CH4 increases be falsified? The Holocene 21, 865-8879. https://doi.org/10.1177/0959683610387172

Ruddiman, W.F., Fuller, D.Q., Kutzbach, J.E., Tzedakis, P.C., Kaplan, J.O., Ellis, E.C., Vavrus, S.J., Roberts, C.N., Fyfe, R., He, F., Lemmen, C., Woodbridge, J., 2016. Late Holocene climate: Natural or anthropogenic ? Rev. Geophys. 54, 93-118. https://doi.org/10.1002/2015RG000503

Sachs, J. P., 2007. Cooling of Northwest Atlantic Slope Waters during the Holocene. Geophysical Research Letters 34 (3): L03609. https://doi.org/10.1029/2006GL028495.

Sànchez-Goñi, M.F., Landais, A., Fletcher, W.J., Naughton, F., Desprat, S., Duprat, J., 2008. Contrasting impacts of Dansgaard-Oeschger events over a western European latitudinal transect modulated by orbital parameters. Quaternary Sc. Rev. 27, 1136–1151. https://doi.org/10.1016/j.quascirev.2008.03.003

Sitzia, L., Bertran, P., Sima, A., Chery, P., Queffelec, A., Rousseau, D.-D., 2017. Dynamics and sources of last glacial aeolian deposition in southwest France derived from dune patterns, grain-size gradients and geochemistry, and reconstruction of efficient wind directions. Quaternary Science Reviews 170, 250–268. https://doi.org/10.1016/j.quascirev.2017.06.029

Sorrel, P., Debret, M., Billeaud, I., Jaccard, S.L., McManus, J.F., Tessier, B., 2012. Persistent non-solar forcing of Holocene storm dynamics in coastal sedimentary archives. Nature Geoscience 5, 892-896. https://doi.org/10.1038/ngeo1619

Steffen, W., Persson, A., Deutsch, L., Zalasiewicz, J., Williams, M., Richardson, K., Crumley, C., Crutzen, P., Folke, C., Gordon, L., Molina, M., Ramanathan, V., Rockström, J., Scheffer, M., Schellnhuber, H.J., Svedin, U., 2011. The anthropocene: from global change to planetary stewardship. Ambio 40(7), 739-761. https://doi.org/10.1007/s13280-011-0185-x

Stéphan, P., Verdin, F., Arnaud-Fassetta, G., Bertrand, F., Eynaud, F., García-Artola, A., Bosq, M., Culioli, C., Suanez, S., Coutelier, C., Bertran, P., Costa, S., 2019. Holocene coastal changes along the Gironde estuary (SW France): new insights from the North Médoc peninsula beach/dune system. Quaternaire 30(1), 47-75. https://doi.org/10.4000/quaternaire.11172

Tastet, J.-P., Pontee, N.I., 1998. Morpho-chronology of coastal dunes in Médoc. A new interpretation of Holocene dunes in Southwestern France. Geomorphology 25, 93–109. https://doi.org/10.1016/S0169-555X(98)00035-X

Tzedakis, P.C., 2010. The MIS 11 – MIS 1 analogy, southern European vegetation, atmospheric methane and the "early anthropogenic hypothesis." Clim. Past, 6, 131–144.

van der Bilt, W.G.M., Bakke, J., Vasskog, K., D'Andrea, W.J., Bradley, R.S., Olafsdottir, S., 2015. Reconstruction of glacier variability from lake sediments reveals dynamic Holocene climate in Svalbard. Quaternary Sc. Rev. 126, 201-218. https://doi.org/10.1016/j.quascirev.2015.09.003

Van Vliet-Lanoe, B., Penaud, A., Henaff, A., Delacourt, C., Fernane, A., Goslin, J., Hallegouet, B., Le Cornec, E., 2014. Middle- to late-Holocene storminess in Brittany (NW France): Part II - The chronology of events and climate forcing. The Holocene 24, 434-453. https://doi.org/10.1177/0959683613519688

Verdin, F., Ard, V., Carrère, I., Eynaud, F., Hoffmann, A., Manen, C., Marchand, G., Saint-Sever, G., 2016. Nouvelles recherches sur le Site de La Lède du Gurp (Grayan-dt-L'hôpital, Gironde) Résultats Préliminaires. 12eme RMPR (Bayonne, 2016) - « Entre deux mers » & Actualité de la Recherche

Verdin, F., Eynaud, F., Stéphan, P., Arnaud-Fassetta, G., Bosq, M., Bertrand, F., Suanez, S., Coutelier, C., Comte, F., Wagner, S., Belingard, C., Ard, V., Manen, C., Saint-Sever, G., Marchand, G., 2019a. Humans and their environment on the Médoc coastline from the Mesolithic to the roman period. Quaternaire 30 (1), 77-75. https://doi.org/10.4000/quaternaire.11201

Verdin, F., López-Romero, E., Eynaud, F., Stéphan, P., 2019b. Les sociétés littorales et leur environnement : l'exemple des recherches interdisciplinaires menées dans le Médoc (Gironde). Les nouvelles de l'archéologie 156. https://doi.org/10.4000/nda.6951

Vinther, B.M., Clausen, H.B., Johnsen, S.J., Rasmussen, S.O., Andersen, K.K., Buchardt, S.L., Dahl-Jensen, D., Seierstad, I.K., Siggaard-Andersen, M.-L., Steffensen, J.P., Svensson, A., Olsen, J., Heinemeier, J., 2006. A synchronized dating of three Greenland ice cores throughout the Holocene. J. Geophys. Res. 111, D13102. https://doi.org/10.1029/2005JD006921

Walker, M., Head, M.J., Lowe, J., Berkelhammer, M., BjÖrck, S., Cheng, H., Cwynar, L.C., Fisher, D., Gkinis, V., Long, A., Newnham, R., Rasmussen, S.O., Weiss, H., 2019. Subdividing the Holocene Series/Epoch: formalization of stages/ages and subseries/subepochs, and designation

of GSSPs and auxiliary stratotypes. J. Quaternary Sci. 34, 173-186. https://doi.org/10.1002/jqs.3097

Waters, C.N., Zalasiewicz, J., Summerhayes, C., Barnosky, A.D., Poirier, C., Ga uszka, A., Cearreta, A., Edgeworth, M., Ellis, E.C., Ellis, M., Jeandel, C., Leinfelder, R., McNeill, J.R., Richter, D. d., Steffen, W., Syvitski, J., Vidas, D., Wagreich, M., Williams, M., Zhisheng, A., Grinevald, J., Odada, E., Oreskes, N., Wolfe, A.P., 2016. The Anthropocene is functionally and stratigraphically distinct from the Holocene. Science 351, https://doi.org/10.1126/science.aad2622

Waters, C.N., Zalasiewicz, J., Summerhayes, C., Fairchild, I.J., Rose, N.L., Loader, N.J., Shotyk, W., Cearreta, A., Head, M.J., Syvitski, J.P.M., Williams, M., Wagreich, M., Barnosky, A.D., An, Z., Leinfelder, R., Jeandel, C., Gałuszka, A., Ivar do Sul, J.A., Gradstein, F., Steffen, W., McNeill, J.R., Wing, S., Poirier, C., Edgeworth, M., 2018. Global Boundary Stratotype Section and Point (GSSP) for the Anthropocene Series: Where and how to look for potential candidates. Earth-Science Reviews 178, 379–429. https://doi.org/10.1016/j.earscirev.2017.12.016

Weiss, H., 2016. Global megadrought, societal collapse and resilience at 4.2–3.9 ka BP across the Mediterranean and west Asia, PAGES Magazine, 24, 62–63.

Zalasiewicz, J., Waters, C., Summerhayes, C., Williams, M., 2018. The Anthropocene. Geology Today 34, 177–181. https://doi.org/10.1111/gto.12244

878 **Figure captions**

879 **Figure 1:** Maps showing the location of the Lède du Gurp (LDG) archaeological site (A): in
880 western Europe; (B): zooming in on the Bay of Biscay margin with other regional marine
881 sequences of interest; (C) Google map view of the residual buttress in the intertidal zone
882 between March and October 2014 before the excavation operations.

883 **Figure 2:** Age-depth relationship (polynomial regression) for the two sampled sequences G3
884 (grey) and G4 (blue). The marks locate the dated samples in depth and time. Dates are calibrated
885 and corrected with CALIB7.0.2. software. The 1σ and 2 σ envelopes (dotted lines) obtained with
886 Undatable software (Lougheed and Obrochta, 2019) are also shown to validate the polynomial
887 construction of age models for G3 and G4, respectively.

888 **Figure 3:** Compilation of sedimentological results obtained for G3 (black curves a, b, c, g, h, i)
889 and G4 (blue curves in b, h) sequences, compared with key pollen data in G3 (d, e, f, j, k).

890 **Figure 4:** Comparison of key results from the G3 and G4 sequences (b, c, d, e, f, g) with some
891 recent Holocene reference records with: (a) bipolar insolation values (June at 60° S and July at
892 65° N) in boreal summers after Berger and Loutre, 1991; (h) Massif central eruptions (total
893 number: attested and supposed) after Miallier et al. 2012; (i) NGRIP $\delta^{18}O$ record after Vinther et
894 al., 2006 and Rasmussen et al., 2006; (j) mean summer SST anomaly in the central eastern
895 Atlantic after de Menocal et al., 2000; (k) mean summer SST anomaly in the southern Bay of
896 Biscay after Eynaud et al. 2018; (l) mean annual SST in the southern Bay of Biscay after Eynaud
897 et al. 2018; (m) global mean temperature reconstruction minus North Atlantic records from
898 Marcott et al. 2013 from the compilation by Marsicek et al. 2018; and (n) CH_4 atmospheric
899 concentration after Beck et al. 2018. Vertical stripes identify sudden short-lived changes in the
900 signals with pink stripes corresponding to warm SST oscillations and light purple stripes to cold

SST. Green boxes at the top identify rapid climate change (RCC) intervals after Mayewski et al., 2004 (temporal limits reproduced from their Figures 1 to 4). Archaeological and climatological divisions commonly used in the North Atlantic region and Europe have been added (after the compilation published in Eynaud et al., 2019 and López-Romero et al., 2021).

Figure 5: Statistical analysis of the XRF results from the G3 sequence, with (a): scores and their significance on PC1 and PC2; (b) ternary plots of key element abundances and (c) their along core distribution (in age) compared to PC1 and PC2 loadings.

Figure 6: Comparison of the respective loadings on PC1 (e) and 2 (f) – and their related key elemental ratio and proxies in LDG (b, d, g, h, j) – with Holocene reconstructions: (a) Arctic glacier activity detected in the sensitive region of Svalbard after normalized titanium loss on ignition (Ti/LOI) measurements in a core from Hajeren Lake (van der Bilt et al. 2015); (c) Atlantic storminess record reconstructed from Danish archives by Goslin et al. (2018a and b); (j) reconstructed sea-surface salinities (SSS) in the Bay of Biscay (PP10-07 core: this work, Mary et al., 2017; Eynaud et al., 2018); (k) SST record from the Scotian margin (after Sachs et al., 2007 and Marsicek et al. 2018) and (l) Dinocyst NAD linked species (% *O. centrocarpum*) in core CBT-CS11 (after Penaud et al., 2020). Vertical stripes: as in Figure 4, the pink stripe corresponds to warm Bay of Biscay SST oscillations and light purple stripes to cold SST. Grey stripes have been added to identify Neoglacial glacier advances in Svalbard after van der Bilt et al. (2015). Archaeological and climatological divisions commonly used in the North Atlantic region and Europe have been added (after the compilation published in Eynaud et al., 2019 and López-Romero et al., 2021).

925 **Table caption**

926 **Table 1:** Age control points (radiocarbon datings) for the Holocene section of the Lède du Gurp
927 (LDG) site.

928

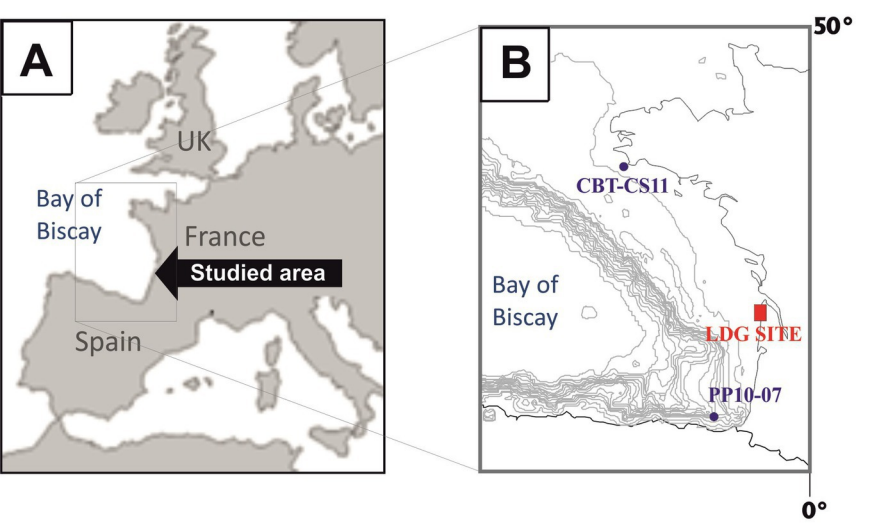
A
UK
Bay of
Biscay
France
Studied area
Spain
B
50°
CBT-CS11
Bay of
Biscay
LDG SITE
PP10-07
0°

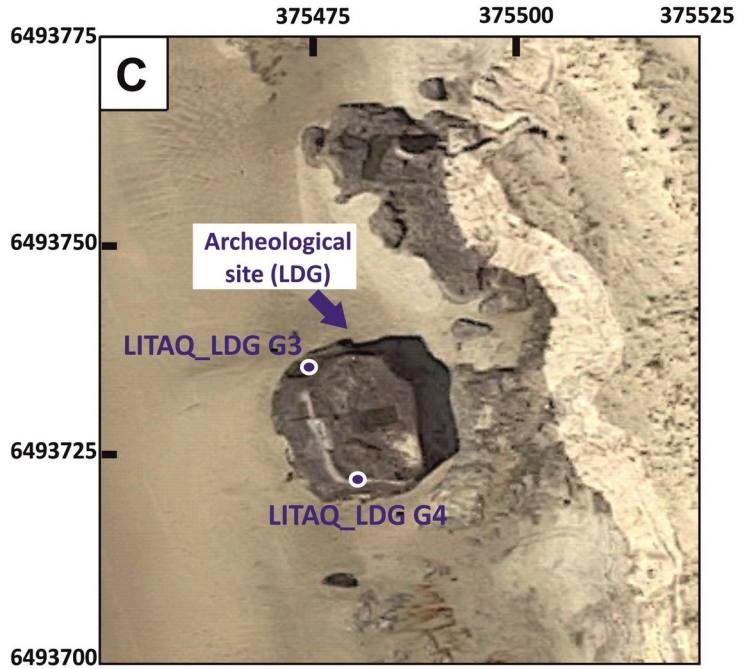
375475
375500
375525
6493775
C
6493750
Archeological
site (LDG)
LITAQ_LDG G3
6493725
LITAQ_LDG G4
6493700

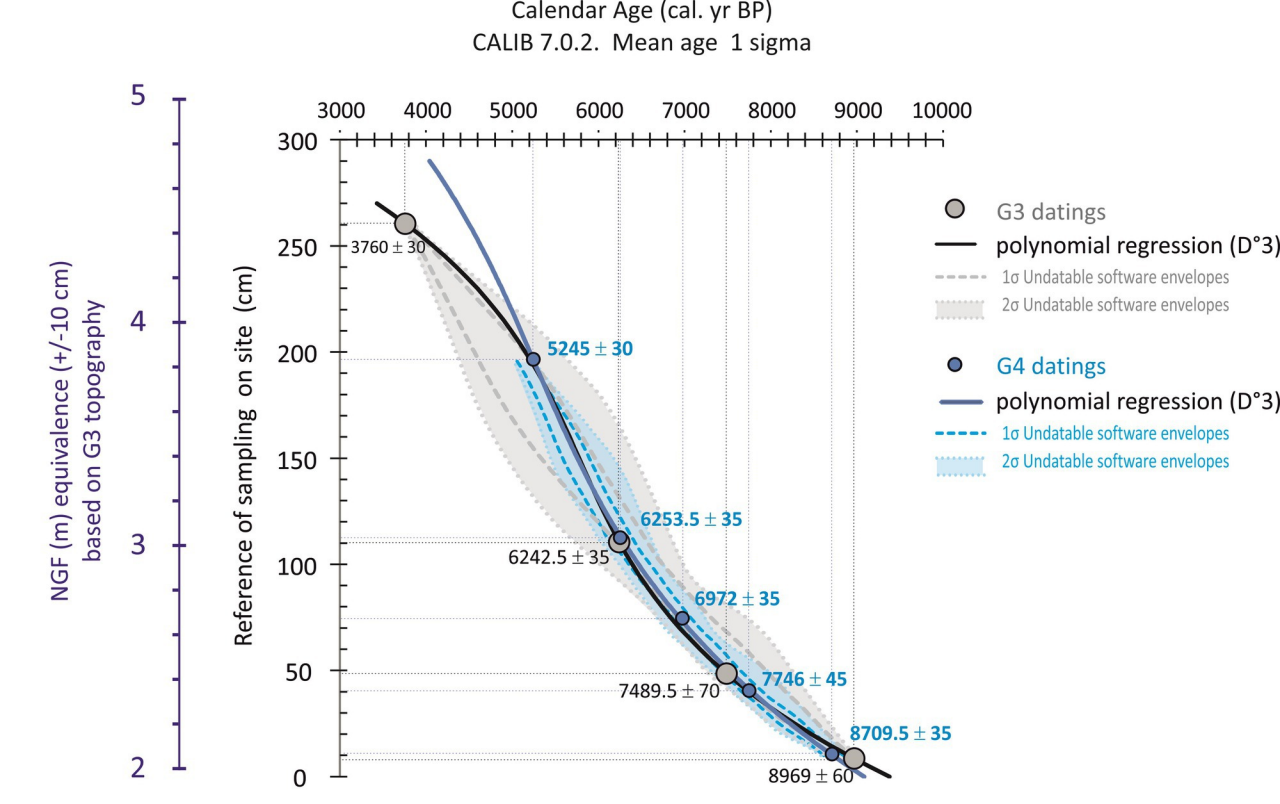
Calendar Age (cal. yr BP)
CALIB 7.0.2. Mean age 1 sigma
3000
4000
5000
6000
7000
8000
9000
10000
Reference of sampling on site (cm)
300
250
200
150
100
50
0
NGF (m) equivalence (+/-10 cm)
based on G3 topography
5
4
3
2
3760 ± 30
5245 ± 30
6253.5 ± 35
6242.5 ± 35
6972 ± 35
7746 ± 45
7489.5 ± 70
8709.5 ± 35
8969 ± 60
G3 datings
polynomial regression (D°3)
1σ Undatable software envelopes
2σ Undatable software envelopes
G4 datings
polynomial regression (D°3)
1σ Undatable software envelopes
2σ Undatable software envelopes

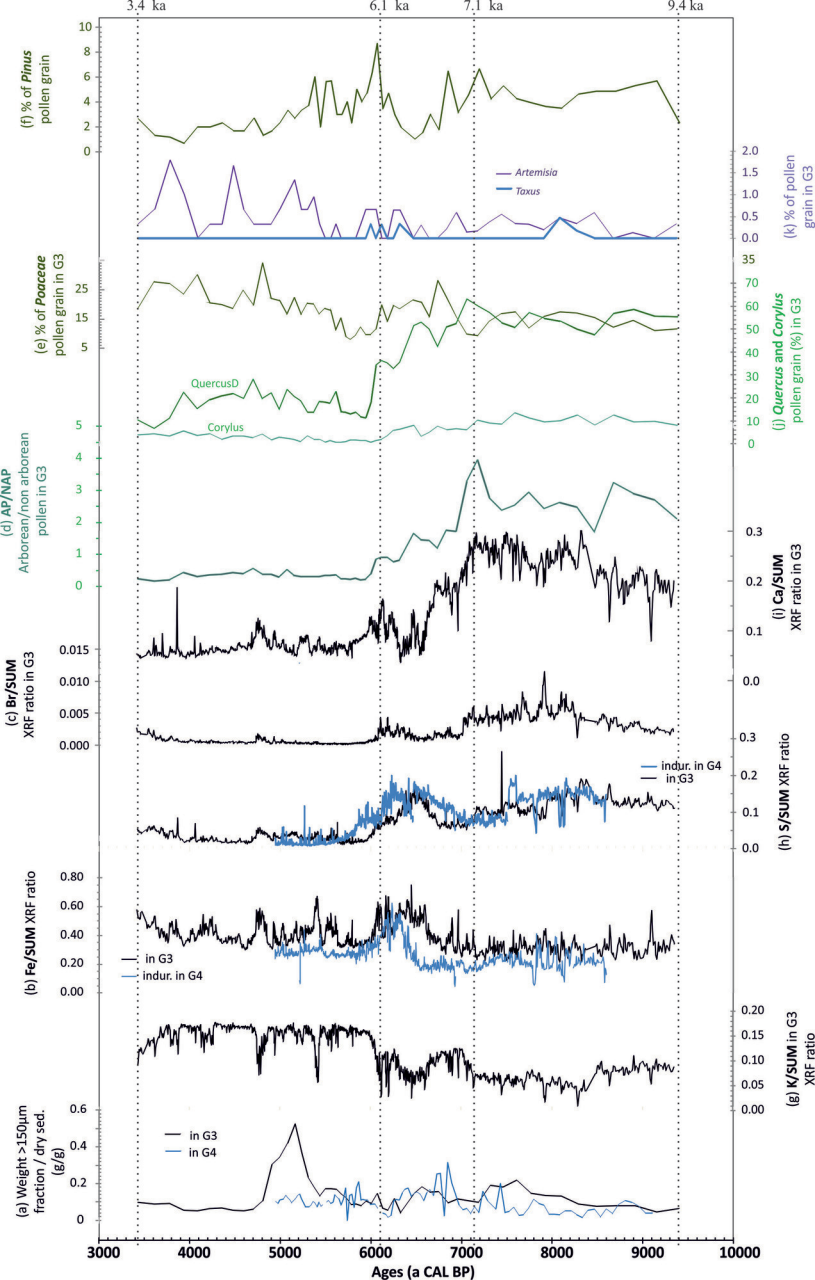
3.4 ka
6.1 ka
7.1 ka
9.4 ka
(f) % of Pinus pollen grain
Artemisia
Taxus
(k) % of pollen grain in G3
(e) % of Poaceae pollen grain in G3
QuercusD
Corylus
(j) Quercus and Corylus pollen grain (%) in G3
(d) AP/NAP Arborean/non arborean pollen in G3
(i) Ca/SUM XRF ratio in G3
(c) Br/SUM XRF ratio in G3
indur. in G4
in G3
(h) S/SUM XRF ratio
(b) Fe/SUM XRF ratio
in G3
indur. in G4
(g) K/SUM in G3 XRF ratio
(a) Weight >150µm fraction / dry sed. (g/g)
in G3
in G4
3000
4000
5000
6000
7000
8000
9000
10000
Ages (a CAL BP)

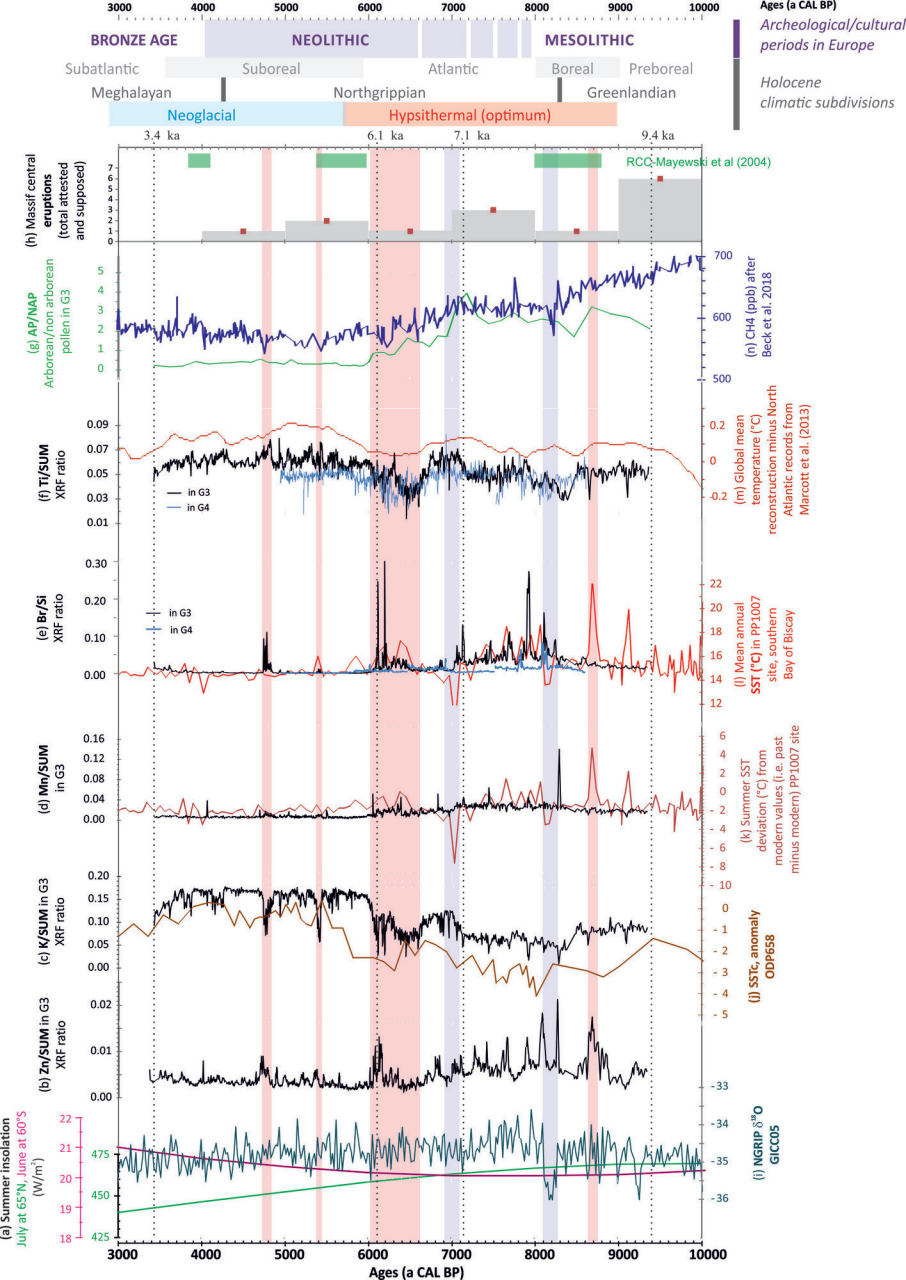
Ages (a CAL BP)
3000 4000 5000 6000 7000 8000 9000 10000
BRONZE AGE
NEOLITHIC
MESOLITHIC
Archeological/cultural periods in Europe
Subatlantic
Suboreal
Atlantic
Boreal
Preboreal
Holocene climatic subdivisions
Meghalayan
Northgrippian
Greenlandian
Neoglacial
Hypsithermal (optimum)
3.4 ka
6.1 ka
7.1 ka
9.4 ka
(h) Massif central eruptions (total attested and supposed)
RCC-Mayewski et al (2004)
(g) AP/NAP Arborean/non arborean pollen in G3
(n) CH4 (ppb) after Beck et al. 2018
(f) Ti/SUM XRF ratio
in G3
in G4
(m) Global mean temperature (°C) reconstruction minus North Atlantic records from Marcott et al. (2013)
(e) Br/Si XRF ratio
(l) Mean annual SST (°C) in PP1007 site, southern Bay of Biscay
(d) Mn/SUM in G3
(k) Summer SST deviation (°C) from modern values (i.e. past minus modern) PP1007 site
(c) K/SUM in G3 XRF ratio
(j) SST$_{UK'37}$ anomaly ODP658
(b) Zn/SUM in G3 XRF ratio
(a) Summer insolation July at 65°N, June at 60°S (W/m²)
(i) NGRIP δ¹⁸O GICC05
Ages (a CAL BP)

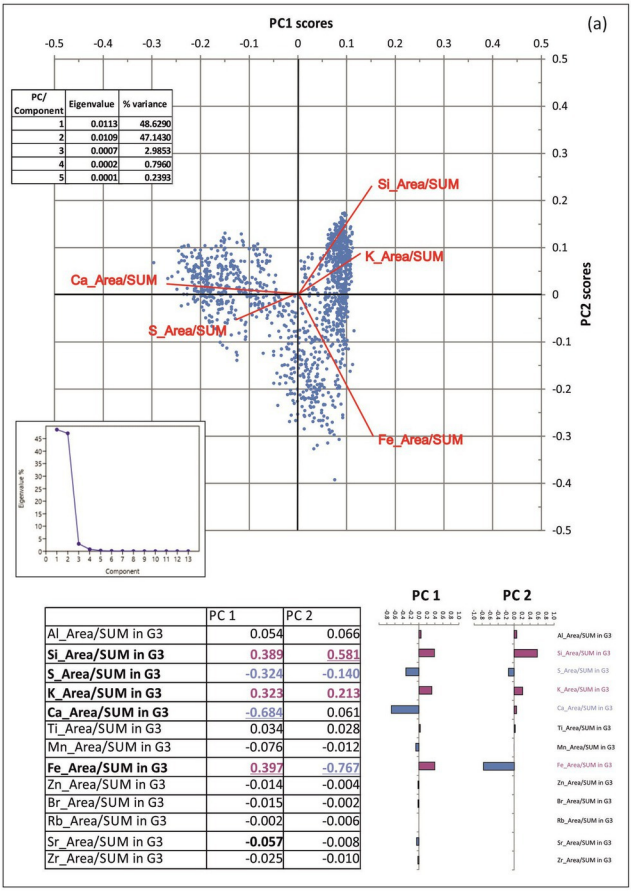

PC/ Component	Eigenvalue	% variance
1	0.0113	48.6290
2	0.0109	47.1430
3	0.0007	2.9853
4	0.0002	0.7960
5	0.0001	0.2393

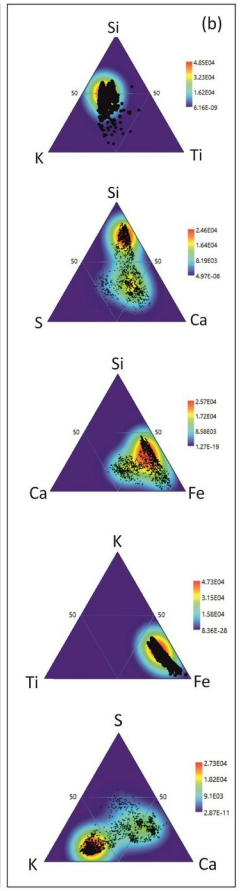

	PC 1	PC 2
Al_Area/SUM in G3	0.054	0.066
Si_Area/SUM in G3	0.389	0.581
S_Area/SUM in G3	-0.324	-0.140
K_Area/SUM in G3	0.323	0.213
Ca_Area/SUM in G3	-0.684	0.061
Ti_Area/SUM in G3	0.034	0.028
Mn_Area/SUM in G3	-0.076	-0.012
Fe_Area/SUM in G3	0.397	-0.767
Zn_Area/SUM in G3	-0.014	-0.004
Br_Area/SUM in G3	-0.015	-0.002
Rb_Area/SUM in G3	-0.002	-0.006
Sr_Area/SUM in G3	**-0.057**	-0.008
Zr_Area/SUM in G3	-0.025	-0.010

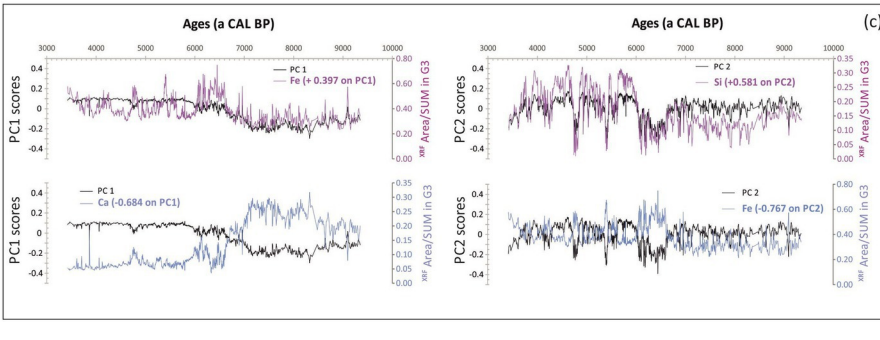

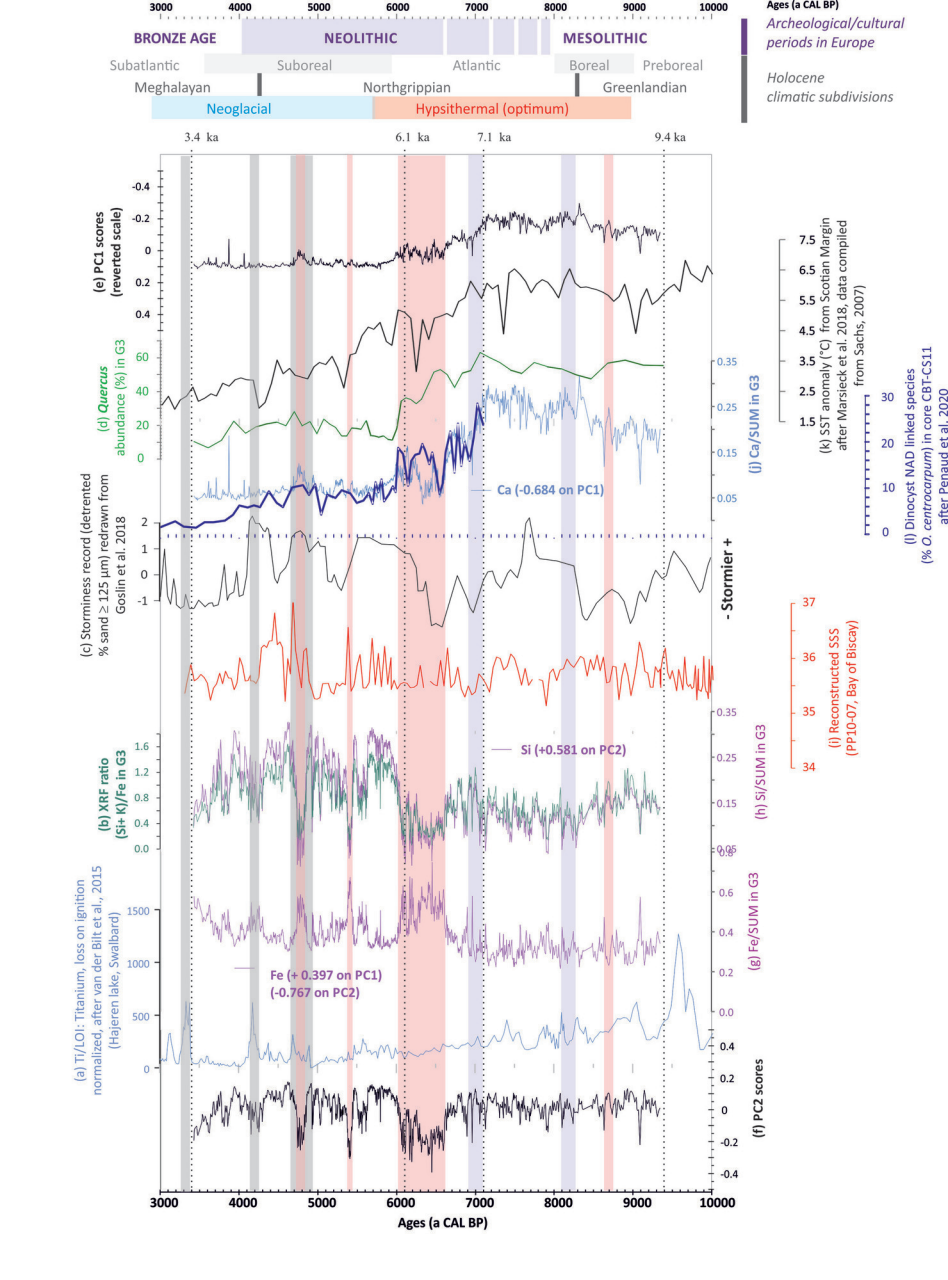
Ages (a CAL BP)
BRONZE AGE
NEOLITHIC
MESOLITHIC
Archeological/cultural periods in Europe
Subatlantic
Suboreal
Atlantic
Boreal
Preboreal
Holocene climatic subdivisions
Meghalayan
Northgrippian
Greenlandian
Neoglacial
Hypsithermal (optimum)
3.4 ka
6.1 ka
7.1 ka
9.4 ka
(e) PC1 scores (reverted scale)
(d) Quercus abundance (%) in G3
(j) Ca/SUM in G3
Ca (-0.684 on PC1)
(k) SST anomaly (°C) from Scotian Margin after Marsieck et al. 2018, data compiled from Sachs, 2007)
(l) Dinocyst NAD linked species (% O. centrocarpum) in core CBT-CS11 after Penaud et al. 2020
(c) Storminess record (detrented % sand ≥ 125 µm) redrawn from Goslin et al. 2018
- Stormier +
(i) Reconstructed SSS (PP10-07, Bay of Biscay)
(b) XRF ratio (Si+ K)/Fe in G3
Si (+0.581 on PC2)
(h) Si/SUM in G3
(a) Ti/LOI: Titanium, loss on ignition normalized, after van der Bilt et al., 2015 (Hajeren lake, Swalbard)
Fe (+ 0.397 on PC1) (-0.767 on PC2)
(g) Fe/SUM in G3
(f) PC2 scores
Ages (a CAL BP)

Field campaign	Sampling references	Mid sampling depth (cm) on site	NGF (m) Equivalent	Material	Lab. code N°	mg C	Delta C13	pMC	Err pMC +/-	Age BP 14c raw	Err age BP +/-	Calendar Age (cal. yr BP) CALIB 7.0.2. One Sigma Ranges: [start	Calendar Age (cal. yr BP) CALIB 7.0.2. One Sigma Ranges: end]	relative area (best score)	Calendar Age (cal. yr BP) CALIB 7.0.2. Mean age 1 sigma	Calendar Age (cal. yr BP) CALIB 7.0.2. Two Sigma Ranges: [start	Calendar Age (cal. yr BP) CALIB 7.0.2. Two Sigma Ranges: end]	relative area (best score)	Calendar Age (cal. yr BP) CALIB 7.0.2. Mean age 2 sigma
LITAQ-2014 -oct	Lède du Gurp, archeological site, Level in G4, slice P1, 10-11 cm	10.5	1.62	seeds	VERA-51390			0.3728	0.0017	7925	35	8640	8779	0.819	8709.5	8628	8813	0.66	8720.5
LITAQ-2014 -oct	Lède du Gurp, archeological site, Level in G4, slice P2, 40-41 cm	40.5	1.93	seeds	VERA-51391			0.4218	0.0023	6935	45	7697	7795	0.939	7746.0	7675	7856	0.98	7765.5
LITAQ-2014 -oct	Lède du Gurp, archeological site, Level in G4, slice P3, 74-75 cm	74.5	2.27	wood	VERA-51392			0.4673	0.0021	6110	35	6927	7017	0.828	6972.0	6892	7032	0.73	6962
LITAQ-2014 -oct	Lède du Gurp, archeological site, Level in G4, slice P4, 112-113 cm	112.5	2.67	seeds	VERA-51393			0.5115	0.0023	5385	35	6231	6276	0.478	6253.5	6173	6284	0.76	6228.5
LITAQ-2014 -oct	Lède du Gurp, archeological site, Level in core G4, P8, 196-197 cm	196.5	3.53	Wood fragments, seeds	SacA-46027	1.59	-28	57.2212	0.1967	4485	30	5211	5279	0.45	5245.0	5038	5293	0.98	5165.5
LITAQ-2014 -oct	Lède du Gurp, archeological site, Levels in G3, P1, 8-9 cm	8.5	2.05	Wood fragments, seeds	SacA-46023	1.36	0.6	36.8652	0.2921	8020	60	8930	9008	0.386	8969	8648	9028	1.00	8838
LITAQ-2014 -oct	Lède du Gurp, archeological site, Level in G3, P2, 48-49 cm	48.5	2.43	Wood roots and fragments, seeds	SacA-46024	1.36	-19.3	43.9439	0.3643	6610	70	7457	7522	0.627	7489.5	7417	7614	1.00	7515.5
LITAQ-2014 -oct	Lède du Gurp, archeological site, Level in G3, P5, 110-111 cm	110.5	3.02	Seeds and Daphnia eggs	SacA-46025	0.93	-22.9	50.9697	0.2087	5415	35	6208	6277	1	6242.5	6179	6293	0.97	6236
LITAQ-2014 -oct	Lède du Gurp, archeological site, Level in G3, P11, 260-261cm	260.5	4.45	Seeds (with Pinus)	SacA-46026	1.78	-19.4	64.6403	0.2391	3505	30	3722	3798	0.813	3760	3695	3861	1.00	3778
FAST LITAQ LDG2017	Lède du Gurp, archeological site, Level in drilling SC1 TR2 47-53 cm	50	-0.55	Wood	SacA-50443	1.26	-31	31.6555	0.1916	9240	50	10372	10498	0.757	10435	10258	10524	0.97	10391